OPEN

Paper

The Methodology Used to Assess Doses from the First Nuclear Weapons Test (Trinity) to the Populations of New Mexico

André Bouville,[1] Harold L. Beck,[2] Kathleen M. Thiessen,[3] F. Owen Hoffman,[3] Nancy Potischman,[4] and Steven L. Simon[1]

Abstract—**Trinity was the first test of a nuclear fission device. The test took place in south-central New Mexico at the Alamogordo Bombing and Gunnery Range at 05:29 AM on 16 July 1945. This article provides detailed information on the methods that were used in this work to estimate the radiation doses that were received by the population that resided in New Mexico in 1945. The 721 voting precincts of New Mexico were classified according to ecozone (plains, mountains, or mixture of plains and mountains), and size of resident population (urban or rural). Methods were developed to prepare estimates of absorbed doses from a range of 63 radionuclides to five organs or tissues (thyroid, active marrow, stomach, colon, and lung) for representative individuals of each voting precinct selected according to ethnicity (Hispanic, White, Native American, and African American) and age group in 1945 (in utero, newborn, 1–2 y, 3–7 y, 8–12 y, 13–17 y, and adult). Three pathways of human exposure were included: (1) external irradiation from the radionuclides deposited on the ground; (2) inhalation of radionuclide-contaminated air during the passage of the radioactive cloud and, thereafter, of radionuclides transferred (resuspended) from soil to air; and (3) ingestion of contaminated water and foodstuffs. Within the ingestion pathway, 13 types of foods and sources of water were considered. Well established models were used for estimation of doses resulting from the three pathways using parameter values developed from extensive literature review. Because previous experience and calculations have shown that the annual dose delivered during the year following a nuclear test is much greater than the doses received in the years after that first year, the time period that was considered is limited to the first year following the day of the test (16 July 1945). Numerical estimates of absorbed doses, based on the methods described in this article, are presented in a separate article in this issue.**
Health Phys. 119(4):400–427; 2020

[1]National Cancer Institute, Bethesda, MD; [2]US Department of Energy (retired); [3]ORRISK, Oak Ridge, TN; [4]National Institutes of Health, Bethesda, MD.

The authors declare no conflicts of interest.

For correspondence contact: André Bouville, 5450 Whitley Park Terrace, Bethesda, MD 20814 or email at **bouvilla@mail.nih.gov**; **ABouville@AOL.com**.

(*Manuscript accepted* 17 *June* 2020).

0017-9078/20/0

DOI: 10.1097/HP.0000000000001331

Key words: dose assessment; fallout; Trinity test; New Mexico

INTRODUCTION

THE TRINITY nuclear test was the culmination of the Manhattan Project that began in 1942 to develop the atomic bomb. The nuclear device that became known as Trinity was designed and fabricated at the Los Alamos Scientific Laboratory in northern New Mexico and tested in south-central New Mexico at the Alamogordo Bombing and Gunnery Range at 05:29 AM on 16 July 1945. Trinity was the first test of a nuclear fission device ever and resulted in the first nuclear explosion. The device simulated the Fat Man type plutonium implosion device used less than 1 month later in the bombing of Nagasaki, Japan.

For the first time, a comprehensive dose assessment of the radiation doses to New Mexico residents resulting from the detonation of the Trinity test has been prepared (Simon et al. 2020). The overall goals and purpose of this work included developing and documenting dose assessment models for the target populations, providing the necessary data for those models, as well as the means to evaluate dosimetric uncertainty for those target populations. Because the NCI Trinity study is a risk projection study (see Cahoon et al. 2020), it is only necessary to estimate doses to representative persons in subgroups in which the dose might be differentiated. This contrasts with other dose reconstructions in which doses must be estimated to identifiable persons.

For our purpose, we have defined the primary target populations, or strata, for dose estimation to be combinations of location, ethnicity, and age. Other determinants of dose [e.g., environment type (ecozones of plains, mountains, etc.) and population density (e.g., urban and rural), as discussed] are modifiers of the basic strata.

Consistent with our goal of estimating doses to representative persons, we provide a strategy and means for estimating uncertainty to the same representative persons. While the form of the methods for estimating uncertainty is like more detailed

studies of individual doses, the purpose here was only to bound the doses to the representative- person doses.

EXPOSURE PATHWAYS CONSIDERED

Estimates of absorbed doses from a range of radionuclides were prepared for representative individuals (I) of the 721 precincts (L) of New Mexico classified according to ethnicity [Hispanic (H), White(W), Native American (NA),[2] and African American (AA)], age group in 1945 (in utero, newborn, 1–2 y, 3–7 y, 8–12 y, 13–17 y, and adult), with some distinctions made for ecozone [plains (P), mountains (M), or mixture of plains and mountains (P/M)], and population density [urban (U) or rural(R)]. For all representative individuals, absorbed doses were estimated for five organs or tissues (thyroid, active marrow, stomach, colon, and lung). These specific organs and tissues were selected because they are expected to give rise to the largest numbers of cancers resulting from radiation exposure to fallout (Simon et al. 2010a): (1) the thyroid gland concentrates radioiodine, which induces thyroid cancer, the predominant health effect investigated in epidemiological studies related to fallout (US DHHS 2005); (2) irradiation of active marrow is expected to increase the risk of leukemia, another health effect investigated in epidemiological studies; (3) stomach and colon are highly exposed after ingestion of fallout because most of the fission products are highly insoluble; and (4) lung is for many fission products the most exposed organ following inhalation of fallout.

Three pathways of human exposure were included: (1) external irradiation, arising mainly from the radionuclides deposited on the ground, and for a small part from radionuclides in the passing cloud; (2) inhalation of radionuclide-contaminated air during the passage of the radioactive cloud and, thereafter, of radionuclides transferred (resuspended) from soil to air; and (3) ingestion of contaminated water and foodstuffs. To the extent possible, well established models were used to calculate the doses resulting from those three pathways.

More than 150 radionuclides were produced in the Trinity test. The 63 radionuclides that were selected for the estimation of the doses from internal irradiation are listed in Table 1. These radionuclides, consisting mostly of fission products, are essentially the same as those previously selected for the study of doses and risks in the Marshall Islands, where 66 tests, many of them thermonuclear, were conducted between 1946 and 1958 (Simon et al. 2010a). The list of 63 selected radionuclides is also generally consistent with those considered in other important fallout studies: (1) the Off-Site Radiation Exposure Review Project (ORERP), which was tasked to estimate the doses from fallout resulting from the nuclear weapons tests that were conducted at the Nevada Test Site (Ng et al. 1990); (2) the US Department of Health and Human Services (US DHHS) assessment of the doses and risks from fallout in the United States from tests conducted worldwide (US DHHS 2005); and (3) the review by the United Nations Scientific Committee on the Effects of Atomic Radiation (UNSCEAR) of the doses arising from fallout at the global scale (UNSCEAR 1993). The exact composition of the fission products generated by a nuclear weapons test depends on the specific fissile nuclide (^{235}U, ^{239}Pu, or ^{238}U) and on the neutron energies involved. Therefore, the composition of the fission products generated by the Trinity test cannot be expected to be the same as those for the tests considered in the other studies. However, the same fission products are generated in either a fission or a thermonuclear test because thermonuclear tests are triggered by the explosion of a fission device, and differences in the distribution of the fission products are mainly observed for products with low fission yield. The selection of 63 radionuclides was deemed to be large enough to include all radionuclides of some importance. Analysis of the dose distributions for the populations of three representative voting precincts in New Mexico presented in a companion paper (Simon et al. 2020) shows that only 38 of the selected radionuclides contributed to 95% of the dose resulting from either external irradiation to all organs and tissues of the body or from internal irradiation to any of the five organs or tissues that were considered.

Among the 63 selected radionuclides, 54 have radioactive half-lives that are less than 3 mo, and only nine have radioactive half-lives longer than 9 mo. Previous studies of NTS fallout have shown that as a result of the preponderance of short-lived radionuclides most of the doses from external irradiation within a few 100 km of the test site are delivered during a few months following a nuclear test (Beck 2005), while the annual doses from internal irradiation are much greater in the year following the test than in any subsequent year (Simon et al. 2010b). Thus, the doses from Trinity were calculated for only the first year following the day of the test (16 July 1945) at all precincts and for all three exposure pathways under consideration (external irradiation, inhalation, and ingestion). These first-year doses also were used in the risk analysis, and the very small doses that were received after the first year were taken to be negligible.

ABSORBED DOSES FROM EXTERNAL IRRADIATION

The absorbed doses from external irradiation, $D_{ext}(I, L)$, in mGy, to representative individual I in precinct L were calculated using the following equation:

$$D_{ext}(I,L) = \frac{K(I)}{24}\left[(X_{out}(L)\ \ T_{out}\ (I)) + (X_{in}\ \ (L)\ \ T_{in}(I))\right] \quad (1)$$

where:

-

[2]The research findings in this paper do not explicitly apply to the people of the Navajo Nation.

Table 1. List[a] and radioactive half-lives of the radionuclides considered in the study.

^{55}Fe (2.7 a)	^{93}Y (10 h)	^{117}Cd (2.5 h)	^{133}I (21 h)	^{147}Nd (11 d)
^{60}Co (5.3 a)	^{95}Zr (64 d)	^{117m}In (2.0 h)	^{135}I (6.6 h)	^{149}Pm (53 h)
^{64}Cu (13 h)	^{95}Nb (35 d)	^{121}Sn (27 h)	^{137}Cs (30 a)	^{149}Nd (1.7 h)
^{77}As (39 h)	^{97}Zr-^{97m}Nb (17 h)	^{125}Sb (2.8 a)	^{139}Ba (83 min)	^{151}Pm (28 h)
^{83}Br (2.4 h)	^{99}Mo (66 h)	^{127}Sn (2.1 h)	^{140}Ba (13 d)	^{153}Sm (46 h)
^{88}Rb (18 min)	^{99m}Tc (6.0 h)	^{127}Sb (3.9 d)	^{140}La (1.7 d)	^{237}U (6.8 d)
^{89}Sr (51 d)	^{103}Ru-^{103m}Rh (39d)	^{129}Sb (4.4 h)	^{141}La (3.9 h)	^{239}Np (2.4 d)
^{90}Sr (29 a)	^{105}Ru (4.4 h)	^{129}Te (70 min)	^{141}Ce (33 d)	^{239}Pu (24,000 a)
^{90}Y (64 h)	^{105}Rh (35 h)	^{131m}Te (30 h)	^{142}La (91 min)	^{240}U (14 h)
^{91}Sr (9.6 h)	^{106}Ru-^{106}Rh (370 d)	^{131}I (8.0 d)	^{143}Ce (33 h)	^{240m}Np (7.4 min)
^{91m}Y (50 min)	^{109}Pd (14 h)	^{132}Te (78 h)	^{143}Pr (14 d)	^{240}Pu (6,600 a)
^{92}Sr (2.7 h)	^{112}Ag (3.1 h)	^{132}I (2.3 h)	^{144}Ce-^{144}Pr (280 d)	
^{92}Y (3.5 h)	^{115}Cd (53 h)	^{133m}Te (55 min)	^{145}Pr (6.0 h)	

[a]The list includes pairs of radionuclides (for example, ^{106}Ru-^{106}Rh) that are treated together because the radioactive half-life of the decay product (^{106}Rh) is much shorter than that of its precursor (^{106}Ru) and the two radionuclides can be considered in radioactive equilibrium for all practical purposes of the study.

K = the conversion coefficient from exposure[3] to dose (mGy mR^{-1}) for representative individual I;

24 = the number of hours in a day;

X_{out} = the outdoor exposure (mR) in precinct L during the first year after the test;

T_{out} = the number of hours spent outdoors in a day by representative individual I;

X_{in} = the indoor exposure (mR) in precinct L during the first year after the test; and

T_{in} = the number of hours spent indoors in a day by representative individual I.

Two types of data are needed to estimate the values of $D_{ext}(I, L)$: (1) the non-radiation data identifying the characteristics of representative individual I, and (2) the radiation data used to estimate the values of the exposure, X_{out} and X_{in}, in each precinct L, as well as the values of the conversion coefficient K from exposure to dose.

Non-radiation data

For each of the 721 precincts (L) of New Mexico, the approximate coordinates (longitude and latitude) of the geographic centroids, a metric of population density [urban (U) or rural (R)], ecozone classification [plains (P), mountains (M), or combination of plains and mountains (P/M)], and the total population in 1945 of each ethnic group were assessed. Population numbers of four ethnic groups [White (W), Hispanic (H), Native American (NA), and African American (AA)] were derived from the New Mexico sections in the US 1940 and 1950 censuses according to seven age groups (in utero, newborn, 1–2 y, 3–7 y, 8–12 y, 13–17 y, and adult). Interpolations and assumptions were needed to convert the census data into the required grouping for our assessment. For example:

- To determine the Urban/Rural status, data from the 1940 and 1950 census for the largest cities and towns in New Mexico were used to estimate the 1945 population of each. Cities/towns with more than 10,000 residents were classified as Urban. Table 2 shows the eight cities/towns and the estimated 1945 populations that were greater than 10,000 persons, which would qualify as urban centers. The population of the eight most populous cities/towns represents about 30% of the state population. Forty-three, or about 6% of the state's 721 voting precincts in 1954, were classified as Urban based on the above scheme. Therefore, 94% of the precincts were classified as Rural;
- The ethnic groups considered in the 1940 and 1950 censuses were identified as: Native White; Foreign born White; Negro; Other races. We assumed that: (1) the white population in our classification corresponded to 58.3% of the Native White + Foreign born White; (2) the Hispanic population in our classification corresponded to 41.7% of the Native White + Foreign born White; (3) the population of Native Americans in our classification corresponded to that identified as Other races; and (4) the population of African Americans in our classification

Table 2. List of urban centers and number of precincts classified as Urban.

County	City/Town	1945 population	Number of precincts classified as Urban
Bernalillo	Albuquerque	66,132	16
Santa Fe	Santa Fe	24,162	9
Chaves	Roswell	19,610	2
Curry	Clovis	13,692	2
San Miguel	Las Vegas	13,063	4
Eddy	Carlsbad	12,546	1
Lea	Hobbs	12,247	2
Doña Ana	Las Cruces	10,355	7
	Sub-total =	171,807	43

[3]Although SI unit for exposure is C kg^{-1}, the traditional unit, mR, is used in this paper to facilitate the comparison with data and results of the 1950s and 1960s.

corresponded to that identified as Negro in the census; and

- In the 1940 and 1950 census, population data are given for 5-y age groups (<5 y, 5 to 10 y, etc.). Those data were interpolated to fit the age distribution selected for the purposes of this paper. See Table 1 of Simon et al. (2020) for the prepared data. In that preparation, we assumed that: (1) the in-utero population was equal to three quarters of the population of infants <1 y of age in 1945; and (2) the age distribution for the entire population of New Mexico was representative of the age distribution of any ethnic group in any ecozone or type of residence.

To determine the number of representative individuals I in each precinct L, consideration was also given to the differences in lifestyle and diet, which depended on variables including ethnicity, ecozone, and population density of the precinct. The primary lifestyle data that have an influence on the absorbed dose from external irradiation are the building materials of the residences and the fraction of time spent in and outdoors. Data from a sample of New Mexico residents alive at the time of Trinity, along with the dietary information, were collected in focus-group meetings and key-informant interviews conducted within the framework of this study with participants classified into 18 possible strata (Table 3) according to ethnicity, ecozone, and type of residence (Potischman et al. 2020). As dietary and lifestyle data for some of the strata were considered to be relatively similar, for our purposes, six data sets (*A*, *B*, *C*, *D*, *E*, and *F*) were derived to describe the population groups of New Mexico (Table 3).

The average values of the lifestyle data obtained from the focus-group meetings and key-informant interviews are presented in Tables 4 and 5:

- Housing construction materials: as indicated in Table 4, adobe and wood were the predominant building materials for the residences in 1945; and
- Time spent outdoors: the values of T_{out} (hours per day) were adjusted to represent the same age groups used in the dose calculation. The results, presented in Table 5 according to data set and age group, show relatively small differences from one data set to another and from one age group to another. These values apply to the summer months, when most of the external dose was delivered and children were out of school.

Table 4. Types of building material used in residences according to data set (Potischman et al. 2020) and corresponding values of the shielding factor.

Data set	Housing construction materials (frequency usage, %)			Shielding factor, *SF*
	Adobe	Wood	Other	
A	78	11	11	0.17
B	91	9	—	0.12
C	73	27	—	0.19
D	50	17	33	0.29
E	—	100	—	0.5
F	100	—	—	0.077

Radiation data

The radiation data that were used to estimate the values of the absorbed doses from external irradiation, $D_{ext}(I,L)$, in mGy, in each precinct L, are: (1) the exposure rates at H + 12 h, in mR h^{-1}, in each precinct; (2) the times of arrival of fallout in each precinct in hours counted from the time of detonation; and (3) the values of the conversion coefficient K from exposure to dose, in mGy per mR, which, in this paper, are taken to only depend on the age group of the representative individual. These radiation data are described in the following paragraphs.

Exposure rates at H+12 h

The values of the outdoor and indoor exposures, X_{out} and X_{in}, cumulated over the first year after the test were derived from data described by isopleths of exposure rates, in units of mR h^{-1}, at 1 m above ground, shown in Fig. 1. The fallout pattern presented in Fig. 1 is adapted from Quinn (1987) and from Cederwall and Peterson (1990). Both studies, which were carried out within the framework of the ORERP, used a methodology that had been developed for the analysis of the nuclear weapons tests conducted at the Nevada Test Site in the 1950s and 1960s (Church et al. 1990). Quinn (1987) performed an analysis of the available exposure-rate data, which, for the most part, were collected during the 3 wk following the Trinity test; the measurements were taken with the help of a variety of instruments, at or near ground level, mainly at populated locations and

Table 3. Data set assignment for each of the 18 strata.

Stratum	Data set	Stratum	Data set	Stratum	Data set	Stratum	Data set
W(U, P)	D	H(U, P)	D	NA(P)	F	AA(U,P)	D
W(U,P/M)	C	H(U,P/M)	C	NA(P/M)	E	AA(U,P/M)	C
W(R, P)	D	H(R, P)	A	NA(M)	E	AA(R, P)	A
W(R, M)	B	H(R, M)	B			AA(R, M)	B
W(R,P/M)	B	H(R,P/M)	B			AA(R,P/M)	B

Table 5. Time spent outdoors (h) per day, according to data set and age group, in summer months (based on Potischman et al. 2020).

Data Set	In utero[a]	Newborn[a]	1–2 y	3–7 y	8–12 y	13–17 y	Adult
A	9	9	10.5	9.3	8.3	8.4	9
B	9	9	10.5	9.3	8.3	8.4	9
C	2	2	13	13	13	8.6	2
D	5	5	5	6.2	7.6	7.1	5
E	10	10	10	10	10	10	10
F[b]	11	11	11	11	11	11	11

[a]The values for "in utero" and "newborn" are taken to be the same as those for the adult.

[b]In addition, 85% of the people in this data set slept on the roof at night.

along roads connecting those populated locations. Cederwall and Peterson (1990) used a meteorological model to expand Quinn's results to areas without available exposure rates in the northern part of the state. Because the measurements of exposure rate were made at various times after the test, they were, as has been done in other fallout studies, normalized by Quinn (1987) to 12 h post-detonation (H +12 h) by means of a multi-exponential function based on calculated radionuclide inventories and exposure rates as a function of time for Trinity (Hicks 1985). In this work, the exposure rate at H+12 is referred to as $\dot{X}(12)$.[4] Because only exposure rates greater that 0.2 mR h^{-1} at H+12 h were considered in Quinn (1987), we added an additional isopleth of 0.1 mR h^{-1} and considered that the exposure rate in any precinct below 0.1 mR h^{-1} was equal to 0.05 mR h^{-1} at H+12 h. This assumption implicitly assigns some degree of exposure to persons living in every precinct of New Mexico in 1945. We note, however, that for most of the state the exposure from Trinity was small compared to the subsequent radiation exposure from NTS and global fallout (Simon et al. 2020). Values of $\dot{X}(12, L)$ for every precinct centroid inside the pattern were obtained by interpolation between isopleths.

Times of arrival of fallout

The radioactive cloud produced by the nuclear detonation extended to an altitude of several kilometers. The nuclear debris, containing a combination of fission and activation products, fell to earth from the different layers of the cloud over a duration which, as a rule of thumb, was on average numerically equal to the initial time of arrival of fallout (Quinn 1990). During the passage of the radioactive cloud over a particular location, the exposure rate at ground level initially began to increase as a result of radioactive decay of the nuclides in the air (descending fallout), followed soon after by the combination of the radioactive decay of descending fallout and of nuclides already deposited on the ground. The exposure rate usually reached a maximum while there was still descending fallout before decreasing to a value at the end of cloud passage over the site that was due only to activity on the ground. The exposure rate decreases after it reaches its maximum primarily because the rapid radioactive decay of nuclides deposited on the ground more than offsets the additional fallout.

Quinn (1987) derived the times of arrival of fallout either from the sequential readings of exposure rate, covering the entire period of descending fallout, which were available for some locations, or, in the absence of such readings, from a meteorological model in which the particle trajectories and fall times were calculated for each layer of the radioactive cloud. The time of maximum rate of fallout, computed using the meteorological model, was defined as the time of arrival of fallout, denoted as *TOA* in this paper. The time of maximum rate of fallout occurs between the time of initial arrival of fallout and the time of peak activity, as observed in the sequential readings of the exposure rate. Within the framework of the ORERP, Quinn (1990) compared the results obtained from the sequential readings of exposure rate and from the meteorological model for several tests conducted at the Nevada Test Site and found reasonable agreement between the two sets of values.

The times of arrival of fallout, counted from the time of detonation at H + 0, were extracted from Quinn (1987) but

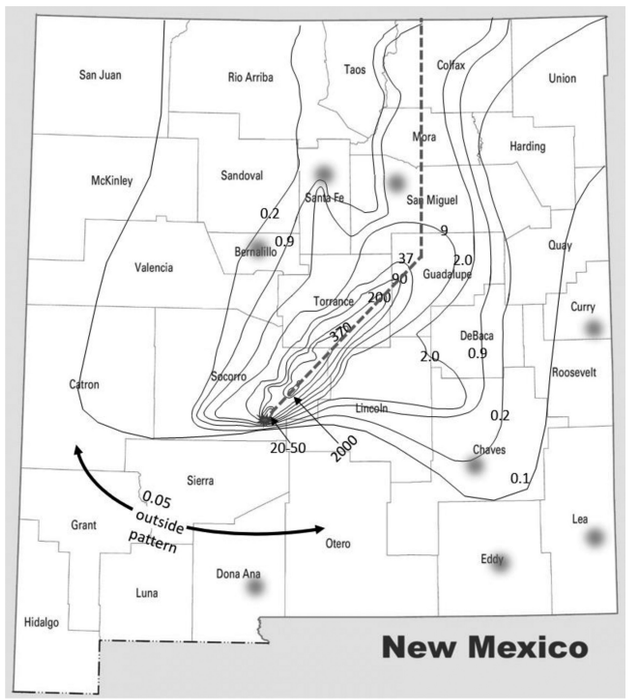

Fig. 1. Map of New Mexico with isopleths of exposure rates (mR h^{-1}) at H+12 h after the test (Quinn 1987; Cederwall and Peterson 1990). These isopleths are derived from measurements of exposure rate conducted during the first few days following the test. Fuzzy spots show the locations of the 8 cities with 1945 populations greater than 10,000. The approximate centerline of the fallout trace is represented by two segments.

[4]In a companion paper (Beck et al. 2020), the exposure rate at H + 12 h is denoted as $E12$. It was also referred to as $\dot{E}R(12)$, $\dot{E}(12)$, $\dot{E}12$, X_E, and X_{12} in other papers related to fallout.

are not shown in Fig. 1. The *TOA* values varied from 0 h at the test site to about 40 h when the main radioactive debris cloud reached the northeast border of New Mexico. In a manner similar to what was done for the exposure rates, we extended, by simple interpolation, the *TOA* values beyond the area of New Mexico considered in Quinn (1987) to assess approximate doses statewide. Values of *TOA(L)* for every precinct centroid inside the pattern were obtained by interpolation between isopleths. Values of *TOA(L)* outside the fallout pattern were assigned values consistent with those obtained for the nearest counties inside the pattern. All precincts of a given county partially or entirely outside the pattern were assigned the same value of *TOA*. Lowest, average, and highest precinct values of $\dot{X}(12)$ and *TOA* from Trinity fallout in each of the 31 counties of New Mexico are presented in Table 6. Because precincts entirely outside the pattern were given the same values of $\dot{X}(12)$ and *TOA*, there is no difference between the lowest, average, and highest values of $\dot{X}(12)$ and *TOA* in those counties.

Table 6. Lowest, average, and highest precinct values of $\dot{X}(12)$ and *TOA* from Trinity fallout in each of the 31 counties of New Mexico.

	$\dot{X}(12)$ (mR h^{-1} at H+12 h)			*TOA* (h)		
County	Lowest	Average	Highest	Lowest	Average	Highest
Bernalillo	0.18	0.37	1.40	8.60	10.2	11.2
Catron	0.05	0.08	0.13	5.30	9.6	12.0
Chaves	0.05	1.30	0.91	15.8	21.3	24.0
Colfax	0.23	1.56	2.0	26.9	33.1	38.0
Curry	0.05	0.06	0.11	18.1	23.4	24.0
De Baca	0.17	1.04	2.48	8.84	12.1	15.5
Dona Ana	0.05	0.05	0.05	24.0	24.0	24.0
Eddy	0.05	0.05	0.05	24.0	24.0	24.0
Grant	0.05	0.05	0.05	24.0	24.0	24.0
Guadalupe	0.86	22.7	104	6.9	10.5	14.1
Harding	0.11	0.16	0.24	23.8	26.2	29.5
Hidalgo	0.05	0.05	0.05	24.0	24.0	24.0
Lea	0.05	0.05	0.05	24.0	24.0	24.0
Lincoln	0.05	8.86	109.6	2.8	13.3	22.0
Luna	0.05	0.05	0.05	24.0	24.0	24.0
McKinley	0.05	0.06	0.12	17.1	23.2	24.0
Mora	0.73	1.58	2.00	17.6	21.6	25.5
Otero	0.05	0.05	0.05	24.0	24.0	24.0
Quay	0.05	0.13	0.29	13.5	21.5	32.0
Rio Arriba	0.12	0.23	0.62	21.0	28.8	38.4
Roosevelt	0.05	0.08	0.13	15.6	22.1	24.0
Sandoval	0.13	0.20	0.53	11.6	16.8	25.6
San Juan	0.05	0.06	0.11	30.8	36.2	39.8
San Miguel	0.26	3.3	19.3	10.0	14.0	20.5
Santa Fe	0.22	1.06	4.14	9.9	15.4	21.4
Sierra	0.05	0.05	0.05	8.0	8.0	8.0
Socorro	0.15	35.5	423	1.0	3.42	6.49
Taos	0.34	0.62	1.04	23.5	29.0	36.5
Torrance	1.3	68.0	481	4.3	6.7	9.1
Union	0.12	0.21	0.71	28.7	35.5	42.4
Valencia	0.05	0.27	1.28	6.19	9.44	12.4

Conversion coefficients *K* from exposure to dose

Photon energies of a few hundred keV are typically emitted by the fission products during their radioactive decay. Based on a similar work related to the nuclear weapons tests conducted in the Marshall Islands (Bouville et al. 2010), the conversion coefficients from exposure to dose for photon energies of a few hundred keV were taken to vary with age but to be independent of the organ or tissue of the body and of the geometry of irradiation (ICRP 2010; NCRP 2018). With respect to the variation with age, the conversion coefficient K was estimated to be 6.6 x 10^{-3} mGy mR^{-1} for adults (Bouville et al. 2010) and to be slightly higher for younger ages (Bellamy et al. 2019; Jacob et al. 1990). The selected values of K for the age groups considered in this study were 6.6 $\times$ 10^{-3} mGy mR^{-1} for the in-utero subjects (same value as for adults), 8.6 $\times$ 10^{-3} mGy mR^{-1} for babies less than 1 y old and for infants less than 3 y, 7.9 $\times$ 10^{-3} mGy mR^{-1} for children aged 3 to 7 y and 8 to 12 y, and 7.3 $\times$ 10^{-3} mGy mR^{-1} for adolescents aged 13 to 17 y.

Outdoor exposure

The outdoor exposure in precinct L, $X_{out}(L)$, in mR, cumulated over the first year after the test, was obtained as:

$$X_{out}(L) = \int_{TOA}^{1\,y} \dot{X}(t,L)\,dt \qquad (2)$$

where *TOA* is the time of arrival of fallout in precinct L, in hours since the detonation, and $\dot{X}(t,L)$ is the exposure rate at time t in precinct L, in mR h^{-1}, which was expressed analytically in the form:

$$\dot{X}(t,L) = \dot{X}(12,L)\sum_{i=1}^{i=10} a\left(\frac{R}{V},i\right) e^{-\lambda\left(\frac{R}{V},i\right)t} \qquad (3)$$

where R/V is the ratio of the total activities of the refractory (R) and of the volatile (V) radionuclides in the radionuclide mix deposited on the ground at *TOA*. For the Trinity test, values of R/V were estimated to range from 0.5 at distances far away from the detonation site to 3 in precincts close to the detonation site (Beck et al. 2020). Detailed information on how R/V was determined for each precinct is discussed by Beck et al. (2020) and is summarized in this paper in the section "Absorbed Doses From Internal Irradiation."

Equation (3) is based on calculated exposure rates, normalized at H + 12 h, for the Trinity test (Hicks 1985). For these calculations, the vertical profile of the activity deposited on the ground was assumed to be exponential with a relaxation length of 0.16 g cm^{-2} to take the surface roughness effects into account (Beck 1980). Exposure rates at 1 m

above the ground surface are provided for the time of detonation (H + 0) and for 30 decay times ranging from 1 h to 50 y. Hicks' results are calculated assuming an instantaneous deposition of fallout at H + 0, whereas the actual conditions after a nuclear detonation involve a combination of descending fallout and of activity depositing on the ground over a relatively extensive length of time. However, comparisons of the calculated results and of the measured exposure rates, either for Trinity (Quinn 1987) or for the tests detonated at the Nevada Test Site (Hicks 1982), show a good agreement for times after the peak activity, probably because the rapid radioactive decay of nuclides deposited on the ground more than offsets the additional fallout. For times preceding the peak activity, the definition of *TOA* being at the maximum rate of fallout results in the inclusion of the exposure due to descending fallout in the calculated exposure arising from the activity deposited on the ground, because the increased calculated exposure between the times of the maximum rate of fallout and of the peak activity is approximately compensated by the elimination of the exposure between the times of initial arrival and maximum rates of fallout. A description of the various ways in which *TOA* could be defined in order to take the descending fallout into account is provided in Thompson et al. (1994).

The values of $a(R/V, i)$ and of $\lambda\ (R/V, i)$, in h^{-1}, for R/V = 0.5 were obtained by fitting the exposure rates (normalized to 1 mR h^{-1} at H+12 h) calculated for 30 times post shot by Hicks (1985). Henderson (1991) fitted Hicks' data for $R/V = 0.5$; Beck (2009) calculated the exposure rates (normalized to 1 mR h^{-1} at H+12 h) for values of $R/V > 0.5$ and fitted those data. The resultant values of $a(R/V, i)$ and of $\lambda\,(R/V, i)$ for R/V equal to 0.5, 1, 1.5, 2, and 3 are presented in Table 7. These fitted values assume only radioactive decay. In the calculations of the exposure rates, we assumed that the activity deposited on the ground varied exponentially with soil depth with a relaxation length of 0.16 g cm^{-2} from the time of deposition at *TOA* until the end of the first year after the test (Hicks 1985; Beck 1980). Weathering of radioactivity into the soil column due to rain will cause the exposure rate to decrease more rapidly than radioactive decay alone, particularly during the several months following the deposition. Since most of the exposure occurred in the first few weeks after the arrival of the fallout, we assumed that weathering in the arid climate of New Mexico would have had a minimal effect on the integral exposure for the first year and have conservatively neglected weathering. Our calculations show that accounting for weathering would decrease the 1-y exposure by about 10% for *TOA* = 4 h and by about 15% for *TOA* = 40 h, for an R/V value of 0.5 in both cases. The variation of R/V from 0.5 to 3 only has a small effect on the 1-y exposure; for example, the 1-y exposures for R/V = 3 would be about 5 and 8% smaller than the corresponding values for R/V=0.5, for *TOA* = 4 and 40 h, respectively.

Indoor exposure

The indoor exposure $X_{in}(L)$, in mR, from *TOA* until 1 y after the test, is calculated as the product of the outdoor exposure $X_{out}(L)$, in mR, and of the shielding factor $SF(L)$:

$$X_{in}(L) = X_{out}(L)\ x\ SF(L). \tag{4}$$

The value of $SF(L)$ varies according to the construction of residences (e.g., brick, adobe, wood, stone or concrete, etc.). The frequency of different housing construction materials, obtained from the focus-group meetings and the individual interviews conducted in New Mexico (Potischman et al. 2020), is shown in Table 4 for each of the six data sets. Adobe and wood were the main housing construction materials in New Mexico in 1945. The shielding factors were taken to be 0.077 for adobe houses (Gordeev et al. 2002) and 0.5 for wooden and other houses, grouped together (Dunning et al. 1957). The average values of the shielding factor for each of the six data sets, considering the mixtures of housing construction materials, are also presented in Table 4.

Organ absorbed doses

The organ absorbed doses from external irradiation [$D_{ext}(L, I)$ in mGy] received by a representative individual I who resided in precinct L during the entire first year after the test are taken to have the same values for the five principal organs and tissues of interest (lung, thyroid, active marrow, stomach, and colon):

$$\begin{aligned} D_{ext}(L,I) &= \frac{K(I)}{24}\ \mathrm{x}\ [(X_{out}(L)\ \mathrm{x}\ T_{out}(I,L)) + (X_{in}(L)\ x\ T_{in}(I,L))] \\ &= \frac{K(I)}{24}\ X_{tot}(I,L) \end{aligned} \tag{5}$$

where

$T_{out}(I,L)$ = the number of hours per day spent outdoors by the considered representative individual I. Its value, which is determined in the data set in which precinct L belongs, depends on the age and ethnicity of the considered representative individual, as well as on the ecozone and type of residence in precinct L. The values of $T_{out}\ (I, L)$ were derived from the focus-group meetings and the individual interviews (Potischman et al. 2020); they are presented in Table 5;

$T_{in}(I,L) = 24\text{-}T_{out}(I,L)$ = the number of hours per day spent indoors by the representative individual I;

$X_{tot}(I,L)$ = the total exposure, in mR, from *TOA* to the end of the first year after the test, associated with the representative individual, I, in precinct L; and

$K(I)$ = the conversion coefficient from exposure to absorbed dose in any organ according to the age of the representative individual, in units of mGy mR^{-1}.

Table 7. Values of the parameters *a(R/V, i)* and *λ(R/V, i)* used to estimate the variation of the exposure rate with time, according to equation 3 (Henderson 1991; Beck et al. 2020).

	Values of *a(R/V, i)*				
R/V =	0.5	1	1.5	2	3
i=1	1.05×10^{2}	1.02×10^{2}	9.75×10^{1}	9.44×10^{1}	9.00×10^{1}
i=2	3.21×10^{1}	3.14×10^{1}	2.64×10^{1}	2.31×10^{1}	1.96 × 101
i=3	2.98×10^{0}	1.64×10^{0}	4.64×10^{0}	4.56×10^{0}	3.04×10^{0}
i=4	7.77×10^{-1}	4.52×10^{0}	4.95×10^{-6}	1.32×10^{0}	9.24×10^{-1}
i=5	2.03×10^{-1}	1.74×10^{-1}	1.46×10^{0}	3.74×10^{-1}	2.53×10^{-1}
i=6	2.38×10^{0}	3.62×10^{-1}	3.92×10^{-1}	1.22×10^{-1}	1.32×10^{-2}
i=7	3.18×10^{-2}	8.11×10^{-2}	7.69×10^{-2}	5.79×10^{-3}	3.00×10^{-3}
i=8	3.45×10^{-3}	8.66×10^{-3}	7.60×10^{-3}	2.84×10^{-2}	8.51×10^{-6}
i=9	2.37×10^{-5}	2.75×10^{-4}	2.21×10^{-5}	2.29×10^{-5}	1.00×10^{-8}
i=10	6.02×10^{-6}	6.41×10^{-6}	1.00×10^{-8}	3.12×10^{-6}	2.57×10^{-6}
	Values of *λ(R/V, i)*				
R/V =	0.5	1	1.5	2	3
i=1	2.00×10^{0}	2.16×10^{0}	2.12×10^{0}	2.09×10^{0}	2.02×10^{0}
i=2	6.84×10^{-1}	7.61×10^{-1}	7.31×10^{-1}	7.06×10^{-1}	6.11×10^{-1}
i=3	6.84×10^{-1}	9.24×10^{-2}	3.22×10^{-1}	3.13×10^{-1}	2.17×10^{-1}
i=4	5.24×10^{-2}	3.37×10^{-1}	5.58×10^{-4}	8.76×10^{-2}	4.78×10^{-2}
i=5	9.79×10^{-3}	3.37×10^{-1}	8.83×10^{-2}	2.26×10^{-2}	9.52×10^{-3}
i=6	1.57×10^{-1}	1.88×10^{-2}	1.87×10^{-2}	8.24×10^{-3}	7.31×10^{-4}
i=7	2.25×10^{-3}	4.33×10^{-3}	4.15×10^{-3}	4.04×10^{-4}	2.08×10^{-3}
i=8	4.14×10^{-4}	6.84×10^{-4}	5.11×10^{-4}	2.57×10^{-3}	1.49×10^{-5}
i=9	1.92×10^{-5}	4.46×10^{-5}	1.24×10^{-5}	2.42×10^{-5}	3.38×10^{-7}
i=10	1.00×10^{-6}	1.40×10^{-6}	3.46×10^{-4}	1.87×10^{-6}	3.76×10^{-6}

Uncertainties in the estimation of the doses from external irradiation

Extensive information on the main sources of uncertainty encountered in the assessment of doses in environmental studies, as well as on the methods that can be used to treat them, is provided in NCRP Reports (NCRP 2007, 2009a and b). In this article, uncertainties in the doses received by each population group in each voting precinct were derived, primarily, from the uncertainties on the estimated exposure rates normalized at H+12 h, i.e., $\dot{X}(12)$. For a given representative individual, *I*, and a given precinct, *L*, the external dose can be expressed as:

$$D_{ext}(I,L) = \dot{X}(12,L) \times \frac{X_{out}(L)}{\dot{X}(12,L)} \times \frac{X_{tot}(I,L)}{X_{out}(L)} \times \frac{D_{ext}(I,L)}{X_{tot}(I,L)}. \quad (6)$$

The uncertainties in individual parameters were assessed to be as follows:

- $\dot{X}(12,L)$: as discussed in Beck et al. (2020), the estimates of $\dot{X}(12)$, in mR h^{-1}, at each precinct centroid were obtained by interpolation of the published fallout pattern (Fig. 1) that was constructed from an analysis of all post-shot monitoring data supplemented by meteorological data (Quinn 1987). Unfortunately, since the monitoring data were limited to areas with roads, the published fallout pattern is itself somewhat uncertain. In addition, the precision and accuracy of $\dot{X}(12)$ vary depending on the accuracy of the instrument used. Therefore, the interpolated values of $\dot{X}(12)$ at each precinct centroid have significant uncertainties. For the purposes of this work, the uncertainty in $\dot{X}(12)$ was assumed to be described by a triangular probability distribution, [TRI(min, mode, max)], as follows. The precincts were classified into three categories: (1) those inside the fallout pattern with a *TOA* less than or equal to 10 h; the uncertainty distribution around the best estimate is TRI (0.33, 1, 3); (2) those inside the fallout pattern, with a *TOA* greater than 10 h; the uncertainty distribution around the best estimate is TRI (0.5, 1, 2); and (3) those outside the fallout pattern, where $\dot{X}(12,L)$ = 0.05 mR h^{-1}; the uncertainty distribution around the best estimate is TRI (0, 1, 1.2);
- $X_{out}(L)/\dot{X}(12,L)$: the uncertainty in the ratio of the outdoor exposure $X_{out}(L)$, in mR, from *TOA* to the end of 1 y after the test, and of the exposure rate at H+12 h, in mR h^{-1}, depends essentially on the uncertainty in *TOA*, which, just like $\dot{X}(12,L)$, was interpolated from the *TOA* pattern published by Quinn (1987). Quinn (1990) estimated that, depending on the nuclear test and on the distance from the test site, TOA could vary from 15 min to several hours. Taking as an example an uncertainty of 30 min for TOA = 1 or 2 h, the uncertainty in the $X_{out}(L)/\dot{X}(12,L)$ ratio would be about 20% for TOA = 1 h and about 10% for TOA = 2 h.

If the uncertainty in TOA is 1 h for TOA = 5 h, the uncertainty in the ratio is about 5%. Other sources of uncertainty include those related to the variation of the outdoor exposure rate with time (model, value of *R/V*, weathering conditions), which are deemed to be minor compared to the uncertainty related to *TOA*. The uncertainty in $X_{out}(L)/\dot{X}(12,L)$ was subjectively taken to be log-normally distributed around the best estimate with a GSD of 1.2 for any precinct, though it is recognized that the uncertainty may be greater at close-in distances than at far away locations;

- $X_{tot}(I,L)/X_{out}(L)$: the uncertainty in the ratio of the total exposure, $X_{tot}(I,L)$, in mR, from *TOA* to the end of the first year, associated with the representative individual, *I*, in precinct, *L*, and of the corresponding outdoor exposure, $X_{out}(L)$, depends on the age, ethnicity, and ecozone of the representative individual. The parameters of interest are the fraction of time spent outdoors, T_{out}, in h d^{-1}, and the shielding factor, *SF*, associated with the building materials used in the residence in 1945. This information was derived from the focus groups and the key informant interviews (Potischman et al. 2020). Based on the variability of the responses provided by the participants of the focus groups and the key informants and taking into account the uncertainties related to the reliability of the responses provided by a small group of persons to represent much larger groups, the uncertainty in $X_{tot}(I,L)/X_{out}(L)$ was subjectively taken to be log-normally distributed around the best estimate with a GSD of 1.3 for any age, ethnicity, and ecozone of the representative individual, in precincts with *TOA* greater than 3 h. For the precincts with *TOA*s less than 3 h (that is, between 05:29 and 08:29 AM on the day of the test), as the age-dependent values of T_{out} may be substantially different from the representative values for the entire day, the GSDs of the log-normal uncertainty distributions around the best estimate were taken to be 1.5; and
- $\frac{D_{ext}(I,L)}{X_{tot}(I,L)} = K(I)$: the uncertainty in $K(I)$, in mGy mR^{-1}, depends on the geometry of irradiation, on the energy spectrum of the incident γ rays, on the organ that is considered, and on the age of the representative individual. In our analysis, only the age of the representative individual was considered in the estimation of the central values of $K(I)$. However, all factors mentioned above were considered in the evaluation of the uncertainty of $K(I)$, which was subjectively estimated to be distributed log-normally around the best estimate with a GSD of 1.2.

The way the uncertainties in the individual parameters were combined to evaluate the uncertainties in the dose estimates is provided in Simon et al. (2020).

ABSORBED DOSES FROM INTERNAL IRRADIATION

The most common and important pathways of internal exposure are ingestion of radioactively contaminated foodstuffs and inhalation of radioactively contaminated air. The doses from internal irradiation (ingestion and inhalation) were derived from the radionuclide-dependent activities estimated to have been deposited at *TOA* on the ground (A_{gd}) or on vegetation (A_{veg}), in Bq m^{-2}, derived directly from outdoor exposure rate, $\dot{X}(12)$, in mR h^{-1} at H + 12 h.

The general expression that was used for the estimation of the internal dose, D_{pw}, in mGy, to an organ, *m*, of a representative individual, *I*, resident of precinct, *L*, from a radionuclide, *Z*, and an exposure pathway, *pw*, was expressed as:

$$D_{pw}(Z,L,I,m) = \dot{X}(12,L) \times \frac{A_{pw}(Z,L,TOA)}{\dot{X}(12,L)} \times \frac{IC_{pw}(Z,L)}{A_{pw}(Z,L,TOA)} \times \frac{Q_{pw}(Z,L,I)}{IC_{pw}(Z,L)} \times \frac{D_{pw}(Z,I,m)}{Q_{pw}(Z,L,I)} \quad (7)$$

where

$A_{pw}(Z, L, TOA)$ = the deposited activity, in Bq m^{-2}, relevant to pathway *pw*, of radionuclide, *Z*, at *TOA*, in precinct *L*;

$IC_{pw}(Z, L)$ = the time-integrated concentration, from *TOA* until 1 y after the test, of radionuclide *Z*, in precinct *L*, in air for inhalation pathways and in the foodstuff of interest for an ingestion pathway. $IC_{pw}(Z, L)$ is expressed in Bq d m^{-3} for inhalation of contaminated air, in Bq d L^{-1} for the ingestion of contaminated water or milk, and in Bq d kg^{-1} for the ingestion of any other contaminated foodstuff of interest;

$Q_{pw}(Z, L, I)$ = the activity intake, in Bq, from *TOA* until one year after the test, of radionuclide *Z*, in air for inhalation pathways and in the foodstuff of interest for an ingestion pathway, by representative individual, *I*, resident of precinct *L*.

The methods used to estimate the values of each term on the right side of the equation, except for $\dot{X}(12,L)$, are discussed in turn.

Normalized activities deposited on the vegetation and on the ground [$A_{pw}/\dot{X}(12, L)$]

The methodology used to estimate the normalized activities deposited on the ground is based on factors and relationships derived by Hicks (1985) for each radionuclide and for a range of TOA values for a mixture of radionuclides corresponding to $R/V = 0.5$. Hicks' values were extended to values of $R/V > 0.5$ by Beck et al. (2020). A model developed in collaboration with Russian scientists was then used to estimate the normalized activities deposited on the ground for values of *R/V* other than 0.5 and also to estimate the

normalized activities deposited on vegetation as a function of *R/V*[5] (Beck 2009; Beck et al. 2020).

Estimation of *R/V*

The radionuclides created during the explosion of a nuclear device are usually classified into refractory or volatile according to whether their melting point is higher or lower than 1,500 °C (Hicks 1982). For example, isotopes of iodine and cesium are classified as volatile, and isotopes of zirconium are classified as refractory (Beck et al. 2010). The variation of *R/V* with location reflects the fact that refractory nuclides condense from the vaporized nuclear debris onto condensation nuclei at earlier times after detonation compared to volatile nuclides and, thus, tend to be incorporated into large particles, i.e., those greater than 50 μm in diameter. Since the larger and more massive particles deposit earlier due to gravitational settling, the earlier the *TOA*, the larger the proportion of large particles deposited and the greater the proportion of total activity deposited that is on large particles, i.e., *R/V* is higher at close-in distances and lower at more distant locations. This phenomenon, termed fractionation, reflects that the *R/V* ratio in the deposited fallout differs from its "unfractionated" value in the debris cloud; that is, without any depletion due to deposition on the ground. Hicks (1982) considered that all elements of a given fission chain, that is, with the same mass number, are either refractory (*R*) or volatile (*V*), except for the chains 91, 140, and 141. For these intermediate chains, the refractory fractions were determined by Hicks (1982) for each chain at 20 s post detonation.[6]

In this analysis, it is only of interest to compare the level of fractionation in each precinct to an unfractionated radionuclide mix. Therefore, the degree of fractionation is expressed as a relative *R/V* ratio, where a ratio of 1.0 represents unfractionated fallout and a ratio of 0.5 represents fallout where one half of the atoms of each refractory radionuclide has been removed, typical of fallout at long distances from the detonation site (Beck et al. 2010; Hicks 1982). Because of the interdependence of fractionation and particle size and because the time of deposition varies for particles of different sizes, use was made of the critical time, T_{cr}, defined as being the time since detonation for all particles greater than 50 μm in diameter, with an assumed density of 2.5 g cm^{-3}, to be deposited. The choice of 50 μm is partly based on the observation from post-detonation test data that in general, only particles of less than approximately 50 μm in diameter were originally retained on vegetation and that the fraction of the total fallout activity that was on small particles at distances close to the detonation site and to the trace axis was very small but increased to 1.0 as one reached distances at which all particles larger than approximately 50 μm would have fallen out by gravitational settling (Lindberg et al. 1959; Larson et al. 1966). For values of TOA ≥ T_{cr}, the relative R/V ratio is equal to 0.5 and all activity deposited will be on particles <50 μm. Even though it is believed that the particle-size distribution and therefore the activity distribution changed with time of deposition post detonation (that is, increased with time for volatile radionuclides and decreased for refractory radionuclides), the crude assumption was made that the activity distribution remained constant (excluding radioactive decay) in locations where *TOA* was greater than, or equal to T_{cr}.

For the Trinity test, the value of T_{cr}, obtained as the quotient of the maximum height of the radioactive cloud, 10.7 km, and of the sedimentation velocity of 50 μm particles, taken to be 0.73 km h^{-1} (Beck et al. 2020), is found to be 14.7 h. Using the joint US–Russian model, described in Beck et al. (2020), the values of *R/V* at the centroids of each precinct *L* were determined from N_{50} (*L*), which is the fraction of total beta activity on particles <50 μm at the time of arrival of fallout (*TOA(L)*):

- for precinct centroids along the axis of the trace of the radioactive fallout, N_{50} (*L*) is denoted as N_{50a} (*L*) and calculated as:

$$N_{50a}(L) = 1 - 0.987\, x\, \exp\left(-d^3\, T_r^3\right) \tag{8}$$

where T_r = *TOA(L)*/T_{cr} and d = 1.6 h^{-1}. This equation, which was developed in association with Russian scientists (Beck et al. 2020), is very similar to that used by Beck et al. (2020), the only difference being in the value selected for *d*, which reflects the spread of the radioactive cloud, and

- for precinct centroids that are off-axis, N_{50} (*L*) is calculated as:

$$N_{50}(L) = N_{50a}(L) - 0.13\, x\, \sqrt{N_{50a}(L)}\ \mathrm{x}\ \ln\left[\dot{X}(12, L)/\dot{X}(12, \mathrm{axis}, L))\right] \tag{9}$$

where $\dot{X}$(12, axis, *L*) is the exposure rate, in mR h^{-1}, at H+12 h along the axis of the trace, at the location where *TOA* = *TOA*(*L*).

It follows from equations 8 and 9 that the value of *R/V* in precinct *L* is derived from the values of *TOA(L)*, $\dot{X}(12, L)$, and $\dot{X}(12, \mathrm{axis}, L)$. Since $\dot{X}(12, L)$ and *TOA(L)* were determined for all precincts, $\dot{X}(12, \mathrm{axis}, L)$ is the only value that remains to be calculated. The variation of $\dot{X}(12, \mathrm{axis}, L)$ along the axis of the trace was estimated using Quinn's fallout pattern as follows:

- The axis of the trace was assumed to consist of two linear segments (Fig. 1): the first segment for the first 10 h after

[5]A peer-reviewed publication on this methodology is under preparation.
[6]For example, if for *R/V* = 1, 40% of the chain is *R* and 60% is *V*, then for *R/V* = 2, the refractory fraction of the chain is multiplied by 2 while the volatile fraction remains the same so that the refractory fraction is now 80% and the volatile fraction 60%. But since the total is now 140%, normalization needs to be done for 100%, resulting in the refractory fraction of this chain for an overall *R/V* = 2 of 57% and in the volatile fraction to be 43%.

the Trinity test, beginning at the detonation site (geographical coordinates: 33.68° N and −106.48° W) and ending at location with coordinates 35.00° N and −104.91° W; and the second one, from 10 to 40 h after the shot, beginning at the end of the first segment (35.00° N, −104.91° W) and ending at 37.00° N, −104.91° W;

- The values of $\dot{X}(12, \text{axis}, L)$ and of $TOA(L)$ were estimated for a number of points along each segment, and the variation of $\dot{X}(12, \text{axis}, L)$ with $TOA(L)$ was fitted using a variety of functions;
- For the first segment, the best fit of the variation with TOA of the exposure rate along the axis, $\dot{X}(12, \text{axis}, L)$, in mR h^{-1}, was obtained, if $TOA(L) < 1.9$ h, as:

$$\dot{X}(12, axis, L) = \text{EXP}\left(4.9\text{–}14.9\ TOA(L)^{2.5} + 13.0\ TOA(L)^{3}\right) \quad (10)$$

and, if 1.9 h ≤ $TOA(L)$ <10 h, as

$$\dot{X}(12, axis, L) = \frac{\left(-128 + 304\ TOA(L)^{2} - 7.2\ TOA(L)^{4} + 0.045\ TOA(L)^{6}\right)}{\left(1 - 0.47\ TOA(L)^{2} + 0.0085\ TOA(L)^{4} - 0.0021\ TOA(L)^{6} + 0.000013\ TOA(L)^{8}\right)} \quad (11);$$ and

- For the second segment, the variation with TOA of the exposure rate along the axis, $\dot{X}(12, \text{axis}, L)$, in mR h^{-1}, was obtained as

$$\dot{X}(12, \text{axis}, L) = 22.8 - 1.9\ TOA(L) + 0.022\ TOA(L)^{2} - 0.0012\ TOA(L)^{3} + 480\ e^{-TOA(L)}. \quad (12)$$

For each precinct L, the value of $N_{50a}(L)$ was determined using the value of $TOA(L)$ in eqn (8). The value of $N_{50}(L)$ was obtained from eqn (9), using the values of $N_{50a}(L)$, $\dot{X}(12, L)$, and $\dot{X}(12, \text{axis}, L)$. Finally, the value of R/V is derived as presented in Table 8 from the value of N_{50a} or N_{50} (Beck et al. 2020). The R/V ratios range from 3 in precincts close to the detonation site to 0.5 at distances where TOA is greater than 14.7 h. Values of $R/V = 0.5$ were found to apply to 667 of the 721 precincts. Values of $R/V > 0.5$ were found for 54 precincts located near the first segment of the axis of the trace (Fig. 1).

The activities of radionuclide (Z) deposited at TOA on ground and vegetation at location (L) depend on the exposure rate $\dot{X}(12, L)$ and on the degree of fractionation (R/V).

Normalized activity of nuclide *Z* deposited on the ground at *TOA* [$A_{gd}/\dot{X}(12)$]

From the model described earlier, the activity of radionuclide Z deposited on the ground at TOA, A_{gd} in Bq m^{-2}, normalized to $\dot{X}(12)$, is expressed as follows:

$$A_{gd}(Z, L, R/V, TOA)/\dot{X}(12, L) = \left(\frac{\beta}{\dot{X}}\right)_{\frac{R}{V},12} (Z/\beta)_{\frac{R}{V},12}\ F_{gd}(Z, TOA) \quad (13)$$

including:

Table 8. Derivation of the values of R/V from those of N_{50} or N_{50a}.

R/V	N_{50a} or N_{50}
0.5	>0.83
1	0.43 – 0.83
1.5	0.23 – <0.43
2	0.09 – <0.23
3	<0.09

$$A_{gd<50}(Z, L, R/V, TOA)/\dot{X}(12, L) = \left(\frac{\beta}{\dot{X}}\right)_{\frac{R}{V},12} N_{50}(L)\ (Z/\beta)_{0.5,12}\ F_{gd}(Z, TOA) \quad (14)$$

where

$A_{gd}(Z,L,R/V,TOA)$ and $A_{gd<50}(Z,L,R/V,TOA)$ = the activity on particles of all sizes and the activity on particles less than 50 μm, respectively, of radionuclide Z deposited on the ground at time TOA (h) at location L (Bq m^{-2}), where the degree of fractionation is R/V;

$\left(\frac{\beta}{\dot{X}}\right)_{\frac{R}{V},12}$ = the ratio of the total β activity deposited on the ground to the exposure rate at H+12 h according to the degree of fractionation R/V (Bq m^{-2} per mR h^{-1}). Selected values of $\left(\frac{\beta}{\dot{X}}\right)_{\frac{R}{V},12}$ are shown in Table 9;

$(Z/\beta)_{\frac{R}{V},12}$ and $(Z/\beta)_{0.5,12}$ = the ratios of the activity of radionuclide Z to the deposited total β activity at time H +12 h, according to R/V, for particles of all sizes ($R/V \neq 0.5$) and for the fraction of particles <50 μm ($R/V = 0.5$), respectively (unitless). Selected values of $(Z/\beta)_{\frac{R}{V},12}$ for the 63 radionuclides under consideration are presented in Table 10, in which (1) all isotopes of Fe, Co, Cu, Zr, Nb, Mo, Tc, Pr, Nd, Pm, Sm, U, Np, and Pu were treated as refractory, as well as ^{142}La, ^{143}Ce, and ^{144}Ce; (2) all isotopes of As, Br, Rb, Ru, Rh, Pd, Ag, Cd, In, Sn, Sb, Te, I, and Cs were treated as volatile, along with ^{90}Sr and ^{90}Y; and (3) ^{91}Sr, ^{91m}Y, ^{140}Ba, ^{140}La, ^{141}La, and ^{141}Ce were treated as intermediate between volatile and refractory (Hicks 1982). The values for ^{239}Pu and ^{240}Pu, considered to be refractory radionuclides, were calculated assuming a ^{240}Pu/^{239}Pu atom ratio of 0.025 and a ^{137}Cs/(^{239}Pu + ^{240}Pu) activity ratio of 30 for $R/V = 0.5$ (Douglas 1978; Beck et al. 2020); and

$F_{gd}(Z, TOA)$ = the value at TOA of the function describing the variation of the activity of radionuclide Z on the ground, normalized to t = 12 h, for the range of TOA values relevant to the Trinity study (1 to 44 h). This function, which is independent of the R/V value, considers the build-up of activity resulting from the radioactive decay of the precursors of radionuclide Z and the loss of activity resulting from the radioactive decay of radionuclide Z.

Table 9. Selected values of the total β activity and of the exposure rate at H+12 h, $\left(\beta/\dot{X}(12)\right)_{\frac{R}{V},12}$, according to the degree of fractionation, *R/V*.

R/V	$\left(\beta/\dot{X}(12)\right)_{\frac{R}{V},12}$ (Bq m^{-2} per mR h^{-1})
0.5	4.11×10^6
1	4.92×10^6
1.5	5.43×10^6
2	5.79×10^6
3	6.24×10^6

Normalized activity of nuclide *Z* deposited on the vegetation at *TOA* [$A_{veg}/\dot{X}(12)$]

The normalized activity of radionuclide *Z* deposited on vegetation at *TOA* at location *L*, $A_{veg}/\dot{X}(12)$, expressed in Bq m^{-2} per mR h^{-1} at H + 12 h, is:

$$\frac{A_{veg}\left(Z,L,\frac{R}{V},\ TOA\right)}{\dot{X}(12,L)} = \frac{A_{gd<50}\left(Z,L,\frac{R}{V},\ TOA\right) f_{dry}}{\dot{X}(12,L)} + \frac{A_{gd}\left(Z,L,\frac{R}{V},\ TOA\right) f_{wet}}{\dot{X}(12,L)} \quad (15)$$

where f_{dry} (unitless) is the fraction of the activity attached to particles <50 μm that is intercepted and initially retained by vegetation as a result from deposition via dry processes. It is calculated according to eqn (16), which is a modification by Vandecasteele et al. (2001) of the original formulation by Chamberlain (1970):

$$f_{dry} = M\left(1-\exp\left(-\alpha\ Y_{dry}\right)\right), \quad (16)$$

where *M* is the maximum interception (unitless), α is the foliar interception constant [m^2 kg^{-1} (dry mass)], and Y_{dry} is the standing crop biomass [kg (dry mass) m^{-2}]. The values of *M* may vary according to the type of vegetation and local plant growth (e.g., row crops vs. pasture with no rows), while the values of α may depend on particle size and chemical form, and the values of Y_{dry} may vary according to the ecozone and the type of vegetation (Thiessen and Hoffman 2018). It is assumed here that the values of α are independent of particle size in the range from 1 to 50 μm. This assumption is based on the summary by Pröhl (2009) of interception measurements obtained from field experiments for dry deposits; in that summary, the interception fractions or the absorption coefficients do not show a clear variation with particle sizes from 1 to 50 μm. The selected values of M, α, and Y_{dry} are:

- M=0.85, α = 2.8, Y_{dry} = 0.3 for vegetables grown in gardens for human consumption;
- M=1, α = 2.8, Y_{dry} = 1 for fruit, berries, etc. directly exposed during fallout; and
- M =1, α = 2.8, Y_{dry} = 0.3 for pasture grasses and other vegetation grazed by cows, sheep, and swine.

f_{wet} is the fraction of the activity attached to particles of all sizes that is intercepted and initially retained by vegetation as a result of deposition via wet processes, that is rainfall, that occurred during the passage of the radioactive cloud at location *L*. Although eqn (16) could also be applied to wet deposition (Kinnersley and Scott 2001), it was considered important to use different models for dry and wet fallout because the main parameters influencing the fraction of the activity that is intercepted and initially retained by vegetation are different in dry and wet conditions. For dry deposition, important factors are particle size, standing biomass, leaf area available for dry deposition, and whether vegetation is dry or wet, whereas for wet deposition important factors are rainfall amount, R in mm, chemical form of the deposit, stage of development of the plant, and its water storage capacity (Pröhl 2009; Hoffman et al. 1992, 1995; Horton 1919). It is essential to note that f_{wet} only applies if the radioactive cloud passes over the location *L* considered at the same time as rain falls. Because rainfall in New Mexico in the summer occurs almost exclusively as transient and short-lived thunderstorms, we have estimated that each local rainfall event might last about 30 min, thus giving the probability of coincidence of the radioactive cloud and the rainfall event at the same time over *L* to be 1/48 ≅ 0.02. This translates to a 98% probability that f_{wet} = 0 and a 2% probability that the value of f_{wet} is in the range from 0 to 1. Recorded daily values of the precipitation, expressed in tenths of millimeter, were collected from the NOAA Global Historical Climatology Network (Menne et al. 2012) for all measuring stations of New Mexico for 16, 17, and 18 July 1945. The recorded values for the day of the test (16 July 1945) are shown on Fig. 2. An interpolation procedure, using inverse distance weighting of the three closest observations within a radius of 0.3° and no spatial correlation other than distance, was used to estimate the daily precipitation at all precincts of New Mexico.

In cases where rainfall occurred during the passage of the radioactive cloud, as assumed in the following calculations, f_{wet} could be calculated (Thiessen and Hoffman 2018) as:

$$f_{wet} = \min(1; LAI \times k \times S/R \times [1-\exp(-R \times \ln(2)/c \times k \times S)] \quad (17)$$

where:

LAI = the leaf area index, a dimensionless quantity that characterizes plant canopies (unitless). It is defined as the one-sided green leaf area per unit ground surface area. *LAI* ranges from 0 (bare ground) to over 10 (dense conifer forests);

k = a unitless constant that quantifies the ability of an element to be attached to the vegetation. Pröhl (2009) proposed values for *k* of 0.5 for anions (Br, I), 1 for monovalent cations (Rb, Cs), and 2 for polyvalent cations (Sr, Ba). The available information for the other elements under consideration (Fe, Co, Cu, As, Y, Zr, Nb, Mo, Tc, Ru, Rh, Pd, Ag, Cd, In, Sn, Sb, Te, La, Ce, Pr, Nd, Pm, Sm, U, Np, Pu) is very sparse; the proposed value for those elements is 1.25,

Table 10. Selected values of the ratios of radionuclide Z and of the deposited total β activity at time H+12 h, according to the degree of fractionation, *R/V*.

Nuclide	*R/V* = 0.5	*R/V* = 1	*R/V* = 1.5	*R/V* = 2	*R/V* = 3
^{112}Ag	2.45×10^{-3}	1.61×10^{-3}	1.20×10^{-3}	9.61×10^{-4}	6.86×10^{-4}
^{77}As	8.99×10^{-5}	5.94×10^{-5}	4.44×10^{-5}	3.55×10^{-5}	2.54×10^{-5}
^{139}Ba	2.45×10^{-3}	1.61×10^{-3}	1.20×10^{-3}	9.61×10^{-4}	6.86×10^{-4}
^{140}Ba	5.74×10^{-3}	4.47×10^{-3}	3.84×10^{-3}	3.46×10^{-3}	3.04×10^{-3}
^{83}Br	2.38×10^{-3}	1.57×10^{-3}	1.17×10^{-3}	9.36×10^{-4}	6.69×10^{-4}
^{115}Cd	4.22×10^{-4}	2.78×10^{-4}	2.08×10^{-4}	1.66×10^{-4}	1.18×10^{-4}
^{117}Cd	3.59×10^{-4}	2.37×10^{-4}	1.77×10^{-4}	1.41×10^{-4}	1.01×10^{-4}
^{141}Ce	1.45×10^{-3}	1.43×10^{-3}	1.43×10^{-3}	1.43×10^{-3}	1.43×10^{-3}
^{143}Ce	2.07×10^{-2}	2.73×10^{-2}	3.06×10^{-2}	3.25×10^{-2}	3.48×10^{-2}
^{144}Ce/^{144}Pr	2.21×10^{-4}	2.92×10^{-4}	3.27×10^{-4}	3.48×10^{-4}	3.72×10^{-4}
^{60}Co	9.00×10^{-7}	1.19×10^{-6}	1.33×10^{-6}	1.41×10^{-6}	1.51×10^{-6}
^{137}Cs	9.90×10^{-6}	5.89×10^{-6}	3.09×10^{-6}	2.18×10^{-6}	1.28×10^{-6}
^{64}Cu	7.23×10^{-3}	9.54×10^{-3}	1.07×10^{-2}	1.14×10^{-2}	1.22×10^{-2}
^{55}Fe	2.16×10^{-7}	2.85×10^{-7}	3.20×10^{-7}	3.40×10^{-7}	3.64×10^{-7}
^{131}I	7.60×10^{-3}	5.01×10^{-3}	3.74×10^{-3}	2.99×10^{-3}	2.13×10^{-3}
^{132}I	2.22×10^{-2}	1.47×10^{-2}	1.09×10^{-2}	8.73×10^{-3}	6.23×10^{-3}
^{133}I	8.73×10^{-2}	5.76×10^{-2}	4.30×10^{-2}	3.43×10^{-2}	2.45×10^{-2}
^{135}I	9.45×10^{-2}	6.23×10^{-2}	4.65×10^{-2}	3.71×10^{-2}	2.65×10^{-2}
^{117m}In	1.04×10^{-3}	6.88×10^{-4}	5.14×10^{-4}	4.10×10^{-4}	2.93×10^{-4}
^{140}La	1.09×10^{-3}	8.47×10^{-4}	7.27×10^{-4}	6.56×10^{-4}	5.76×10^{-4}
^{141}La	4.26×10^{-2}	4.21×10^{-2}	4.20×10^{-2}	4.19×10^{-2}	4.19×10^{-2}
^{142}La	3.19×10^{-3}	4.20×10^{-3}	4.70×10^{-3}	5.00×10^{-3}	5.36×10^{-3}
^{99}Mo	1.59×10^{-2}	2.10×10^{-2}	2.35×10^{-2}	2.50×10^{-2}	2.68×10^{-2}
^{95}Nb	6.23×10^{-6}	8.21×10^{-6}	9.20×10^{-6}	9.78×10^{-6}	1.05×10^{-5}
^{147}Nd	1.71×10^{-3}	2.25×10^{-3}	2.52×10^{-3}	2.69×10^{-3}	2.88×10^{-3}
^{149}Nd	1.56×10^{-3}	2.05×10^{-3}	2.30×10^{-3}	2.45×10^{-3}	2.62×10^{-3}
^{239}Np	2.12×10^{-1}	2.80×10^{-1}	3.14×10^{-1}	3.34×10^{-1}	3.57×10^{-1}
^{240m}Np	4.44×10^{-3}	5.86×10^{-3}	6.56×10^{-3}	6.98×10^{-3}	7.48×10^{-3}
^{109}Pd	7.89×10^{-3}	5.20×10^{-3}	3.88×10^{-3}	3.10×10^{-3}	2.21×10^{-3}
^{141}Pm	4.71×10^{-3}	6.21×10^{-3}	6.95×10^{-3}	7.39×10^{-3}	7.92×10^{-3}
^{151}Pm	4.36×10^{-3}	5.76×10^{-3}	6.45×10^{-3}	6.86×10^{-3}	7.34×10^{-3}
^{143}Pr	5.71×10^{-4}	7.54×10^{-4}	8.44×10^{-4}	8.98×10^{-4}	9.61×10^{-4}
^{145}Pr	2.74×10^{-2}	3.62×10^{-2}	4.05×10^{-2}	4.31×10^{-2}	4.62×10^{-2}
^{239}Pu	3.16×10^{-7}	4.15×10^{-7}	4.67×10^{-7}	5.09×10^{-7}	5.41×10^{-7}
^{240}Pu	2.88×10^{-8}	3.78×10^{-8}	4.26×10^{-8}	4.64×10^{-8}	4.93×10^{-8}
^{88}Rb	1.25×10^{-2}	8.25×10^{-3}	6.16×10^{-3}	4.91×10^{-3}	3.51×10^{-3}
^{105}Rh	3.64×10^{-2}	2.40×10^{-2}	1.79×10^{-2}	1.43×10^{-2}	1.02×10^{-2}
^{103}Ru/^{103m}Rh	2.65×10^{-3}	1.75×10^{-3}	1.31×10^{-3}	1.04×10^{-3}	7.44×10^{-4}
^{105}Ru	6.19×10^{-2}	4.08×10^{-2}	3.05×10^{-2}	2.43×10^{-2}	1.74×10^{-2}
^{106}Ru/^{106}Rh	3.58×10^{-4}	2.36×10^{-4}	1.76×10^{-4}	1.41×10^{-4}	1.00×10^{-4}
^{125}Sb	1.06×10^{-6}	7.03×10^{-7}	5.26×10^{-7}	4.20×10^{-7}	3.00×10^{-7}
^{127}Sb	1.53×10^{-3}	1.01×10^{-3}	7.53×10^{-4}	6.01×10^{-4}	4.29×10^{-4}
^{129}Sb	1.67×10^{-2}	1.10×10^{-2}	8.24×10^{-3}	6.57×10^{-3}	4.69×10^{-3}
^{153}Sm	1.48×10^{-3}	1.95×10^{-3}	2.18×10^{-3}	2.32×10^{-3}	2.48×10^{-3}
^{121}Sn	8.18×10^{-4}	5.39×10^{-4}	4.03×10^{-4}	3.21×10^{-4}	2.29×10^{-4}
^{127}Sn	5.63×10^{-4}	3.71×10^{-4}	2.77×10^{-4}	2.21×10^{-4}	1.58×10^{-4}
^{89}Sr	9.06×10^{-4}	5.43×10^{-4}	4.05×10^{-4}	3.23×10^{-4}	2.31×10^{-4}
^{90}Sr	4.44×10^{-6}	2.66×10^{-6}	1.99×10^{-6}	1.59×10^{-6}	1.13×10^{-6}
^{91}Sr	4.61×10^{-2}	3.59×10^{-2}	3.01×10^{-2}	2.67×10^{-2}	2.29×10^{-2}
^{92}Sr	1.12×10^{-2}	1.48×10^{-2}	1.66×10^{-2}	1.77×10^{-2}	1.89×10^{-2}
^{99m}Tc	1.09×10^{-2}	1.44×10^{-2}	1.61×10^{-2}	1.71×10^{-2}	1.83×10^{-2}

Continued next page

Table 10. *(Continued)*

Nuclide	$R/V = 0.5$	$R/V = 1$	$R/V = 1.5$	$R/V = 2$	$R/V = 3$
^{129}Te	1.90×10^{-2}	1.25×10^{-2}	9.35×10^{-3}	7.46×10^{-3}	5.32×10^{-3}
^{131m}Te	4.87×10^{-3}	3.21×10^{-3}	2.40×10^{-3}	1.91×10^{-3}	1.37×10^{-3}
^{132}Te	2.15×10^{-2}	1.42×10^{-2}	1.06×10^{-2}	8.45×10^{-3}	6.03×10^{-3}
^{133m}Te	4.15×10^{-5}	2.74×10^{-5}	2.04×10^{-5}	1.63×10^{-5}	1.16×10^{-5}
^{237}U	1.37×10^{-2}	1.80×10^{-2}	2.02×10^{-2}	2.15×10^{-2}	2.30×10^{-2}
^{240}U	4.40×10^{-3}	5.81×10^{-3}	6.50×10^{-3}	6.91×10^{-3}	4.58×10^{-3}
^{90}Y	5.47×10^{-7}	3.62×10^{-7}	2.71×10^{-7}	2.16×10^{-7}	1.54×10^{-7}
^{91m}Y	2.96×10^{-2}	2.30×10^{-2}	1.93×10^{-2}	1.71×10^{-2}	1.47×10^{-2}
^{92}Y	3.89×10^{-2}	5.13×10^{-2}	5.74×10^{-2}	6.11×10^{-2}	6.54×10^{-2}
^{93}Y	3.64×10^{-2}	4.79×10^{-2}	5.37×10^{-2}	5.71×10^{-2}	6.12×10^{-2}
^{95}Zr	6.55×10^{-4}	8.64×10^{-4}	9.67×10^{-4}	1.03×10^{-3}	1.10×10^{-3}
^{97}Zr/^{97m}Nb	3.66×10^{-2}	4.83×10^{-2}	5.41×10^{-2}	5.75×10^{-2}	6.16×10^{-2}

with a uniform probability distribution from 0 to 2.5 (Thiessen and Hoffman 2018);

S = the water storage capacity of the plant (mm). Pröhl (2009) proposed values for S of 0.2 mm for grass, cereals, and corn (maize), and of 0.3 mm for all other crops;

R = the total amount of rain during a single event (mm), and

c = a unitless constant dependent on the type of plant and ambient conditions (e.g., rainfall intensity and wind speed). Thiessen and Hoffman (2018) proposed a log-triangular probability distribution with a mode of 3 and lower and upper bounds of 0.5 and 5, respectively.

Fig. 2. Map of recorded precipitation, expressed in tenths of millimeters per day, on 16 July 1945 in all measuring stations of New Mexico (derived from the Global Historical Climatology Network–Daily Database; Menne et al. 2012).

Variation with time of the normalized activities of nuclide *Z*

The variation with time of the normalized activities of radionuclide Z deposited on the ground and on vegetation was calculated using the normalized values for the Trinity test provided by Hicks (1985) for a range of times during the first year after the test. When needed, account was taken of the environmental removal processes. For most radionuclides, the variation with time was expressed with simple exponentials. More complex analytical expressions were used when the radionuclide Z had a radioactive precursor produced by fission and radioactive equilibrium was not reached during the first few minutes after the shot. This was the case for ^{112}Ag, ^{77}As, ^{141}Ce, ^{131}I, ^{117m}In, ^{140}La, ^{95}Nb, ^{239}Np, ^{149}Pm, ^{105}Rh, ^{125}Sb, ^{99m}Tc, ^{90}Y, ^{91m}Y, and ^{92}Y.

Normalized time-integrated concentrations in air and foodstuffs (IC_{pw}/A_{pw})

Normalized time-integrated concentrations in air were considered for two inhalation pathways: acute inhalation during the passage of the radioactive cloud and protracted inhalation from resuspension of deposited activity, for example during windstorm events, in the first year after the test.

The ingestion pathways include the consumption of drinking water and of eight foodstuffs, namely leafy vegetables, fruit vegetables, fruit and berries, cow's milk, cow cheese, beef, mutton, and pork. The consumption of goats' milk was also considered in the dietary survey; however, it was reported so infrequently that it could not be assumed or quantified on a population basis (Potischman et al. 2020). The origin of the contamination of all foodstuffs is the fallout deposition on plant leaves during the cloud passage. The normalized time-integrated concentrations correspond to the food products consumed, considering the time delay between production and consumption, as well as the changes in concentrations due to the culinary preparation of the foodstuffs. In the absence of detailed information on local or regional patterns of foodstuffs other than cow's

milk, those foodstuffs were assumed to have been produced in the same precinct in which they were consumed.

The inhalation pathways are discussed first.

Inhalation during the passage of the cloud

The method used to estimate the time-integrated concentrations in ground-level air during the passage of the cloud is the same as in Simon et al. (1990). In the absence of measured air concentrations, their values were derived using the relationship proposed by Chamberlain and Chadwick (1953) between the dry deposition flux and the air concentration. The ratio of the two quantities, termed deposition velocity, is equal to the ratio of the deposition density and of the time-integrated concentrations in air. The dry deposition values have been reported to range over three orders of magnitude as they vary according to micrometeorological variables (e.g., atmospheric stability, temperature, and wind velocity), properties of the depositing material (e.g., particle size and solubility), and surface variables (e.g., canopy growth and structure) (Sehmel et al. 1980). Therefore, there are substantial difficulties in determining suitable deposition-velocity values, as the values of many influencing parameters may be unknown. Despite the difficulties associated with the determination of the appropriate deposition velocity, the relationship proposed by Chamberlain and Chadwick (1953) is generally used to estimate the inhalation dose in the absence of measured air concentrations, and it was, for example, used in two studies related to fallout from tests detonated at the Nevada Test Site (NCI 1997; Simon et al. 1990).

The method proposed by Simon et al. (1990) also takes into consideration the facts that the average particle size decreases as *TOA* increases and that the large particles are not respirable, i.e. cannot penetrate deep into the lung. Because the Trinity test occurred in the summer before indoor air conditioning was widely available, we assumed that the buildings were naturally ventilated without filtration by open windows, and so the air concentrations indoors were approximately equal to those outdoors. In brief, the relationship between the deposited activity on the ground, A_{gd}, and the time-integrated concentration of the respirable-sized particles in air, IC_{cd} in Bq s m^{-3}, was estimated to be (Simon et al. 1990):

$$IC_{cd}(Z,L) = \frac{A_{gd}\left(Z,L,\frac{R}{V},TOA\right)}{v_d}\, x\, f_{or}(TOA), \quad (18)$$

where:

f_{or} is the fraction of the time-integrated air concentration on particles of respirable sizes, taken to be 10 μm or less. Simon et al. (1990) derived a function based on time of arrival of fallout, *TOA* in hours, based on Nevada test data. For Trinity, however, we estimated f_{or} to be somewhat smaller and to vary from 0.08 to 0.2, depending on distance; and

v_d is the average deposition velocity, expressed in m s^{-1}, for particles <10 μm. For Trinity, we found v_d to be about 2 10^{-3} m s^{-1}, as estimated from Sehmel (1980) for particles of about 5 μm diameter (midpoint of the respirable range).

Inhalation dose due to resuspended material

The time-integrated concentrations in ground-level air, in Bq d m^{-3}, due to resuspension during the first year after the test, $IC_{res}(Z,L)$, were derived from measured values of the resuspension factor $S_f(t)$, which is the ratio of the air concentration and of the deposited activity (Anspaugh et al. 2002; Maxwell and Anspaugh 2011):

$$IC_{res}(Z,L) = \int_{TOA}^{365} A_{gd}\left(Z,L,\frac{R}{V},t\right) S_f(t)\, dt \quad (19)$$

where the resuspension factor $S_f(t)$, in m^{-1}, is expressed as:

$$S_f(\mathrm{t}) = 10^{-5}\, \mathrm{e}^{-0.07\, t} + 7\ 10^{-9}\, \mathrm{e}^{-0.002\, t} + 10^{-9} \quad (20)$$

where the time t after deposition at *TOA* is expressed in days.

For a radionuclide Z with no significant input of a precursor after *TOA* and a radioactive decay constant, λ in d^{-1}, the activity deposited on the ground varies as:

$$A_{gd}\,(Z,L,R/V,t) = A_{gd}\,(Z,L,R/V,TOA)\ \mathrm{e}^{-\lambda\,(t-TOA)} \quad (21)$$

and the time-integrated concentration in air from $t_1 = TOA$ to $t_2 = 365$ d is obtained as:

$$IC_{res}(Z,L) = A_{gd}\left(Z,L,\frac{R}{V},TOA\right)\left[\frac{10^{-5}}{0.07+\lambda}\left(e^{-(0.07+\lambda)\,t_1}\right) - e^{-(0.07+\lambda)\,t_2}\right) + \frac{7\ 10^{-9}}{0.002+\lambda}\left(\mathrm{e}^{-(0.002+\lambda)\,t_1}\right) - \mathrm{e}^{-(0.002+\lambda)\,t_2}\right) + \frac{10^{-9}}{\lambda}\left(\mathrm{e}^{-(\lambda)\,t_1} - \mathrm{e}^{-(\lambda)\,t_2}\right)\Big]. \quad (22)$$

For a radionuclide Z with a radioactive precursor produced by fission, dp, with a radioactive decay constant, λ_{dp} in d^{-1}, the activity of the decay product deposited on the ground varies as:

$$A_{gd}\,(dp,L,R/V,t) = A_{gd}\,(Z,L,R/V,TOA)\ x\ \left(\lambda_{dp}/\left(\lambda_{dp}-\lambda\right)\right)\ x\ \left(\exp(-\lambda\ t) - exp\left(-\lambda_{dp}\ t\right)\right) + A_{gd}(dp,L,R/V,TOA)\ x\ \exp\left(-\lambda_{dp}\ t\right) I \quad (23)$$

and the time-integrated concentration in air from $t_1 = TOA$ to $t_2 = 365$ d is obtained as:

$$
\begin{aligned}
&IC_{res}\,(dp, L)\\
&= A_{gd}\,(Z, L, R/V, TOA)\; x\; \left(\lambda_{dp}/\left(\lambda_{dp}-\lambda\right)\right)\; x\; \left(10^{-5}/(0.07+\lambda)\right)\; x\\
&\quad (\exp(-(0.07+\lambda)\,t_1)-\exp(-0.07+\lambda)t_2))-\left(10^{-5}/\left(0.07+\lambda_{dp}\right)\right)\; x\\
&\quad \left(\exp\left(-\left(0.07+\lambda_{dp}\right)\,t_1\right)-\exp\left(-0.07+\lambda_{dp}\right)t_2\right))\\
&\quad +\left(7\times10^{-9}/(0.002+\lambda)\right)\; x\; \exp(-(0.002+\lambda)\,t_1)-\exp(-0.002+\lambda)t_2))\\
&\quad -\left(\left(7\times10^{-9}/0.002+\lambda_{dp}\right)\right)\; x\; \left(\exp-\left(0.002+\lambda_{dp}\right)\,t_1\right)-\exp\left(-0.002+\lambda_{dp}\right)t_2))\\
&\quad +\;\left(\left(10^{-9}/\lambda\right)\; x\; \exp(-\lambda\; t_1)-\exp(-\lambda\; t_2)\right)-\left(\left(10^{-9}/\lambda_{dp}\right)\right.\\
&\quad x\; \left(\exp\left(-\lambda_{dp}\; t_1\right)-\exp\left(-\lambda_{dp}\; t_2\right)\right)\left.\right)]+A_{gd}\;(dp, L, R/V, TOA)\\
&\quad x\; [\left(\left(10^{-5}/\left(0.07+\lambda_{dp}\right)\right)\; x\; \left(\exp\left(-\left(0.07+\lambda_{dp}\right)\,t_1\right)-\exp\left(-0.07+\lambda_{dp}\right)t_2\right)\right)\\
&\quad +\left(\left(7\;x\;10^{-9}/0.002+\lambda_{dp}\right)\right)\\
&\quad x\; \left(\exp\left(-\left(0.002+\lambda_{dp}\right)\,t_1\right)-\exp\left(-0.002+\lambda_{dp}\right)t_2\right))\\
&\quad +\left(\left(10^{-9}/\lambda_{dp}\right)\; x\; \left(\exp\left(-\lambda_{dp}\; t_1\right)-\exp\left(-\lambda_{dp}\; t_2\right)\right)\right)]\}I. \qquad (24)
\end{aligned}
$$

Ingestion of drinking water

Drinking water from cisterns, wells, public network, rivers, and acequias (or "irrigation ditches") could have been contaminated with radioactive fallout from the Trinity test. The following assumptions were made regarding the origin of the drinking water:

- Tap water was derived from a river that flowed in 331 precincts (Fig. 3), including all precincts where main towns and cities are located;
- Cisterns and wells provided water for the other precincts with 50% of the consumption of drinking water in those precincts assumed to originate from cisterns, and the other 50% from wells; and
- Acequias, i.e., irrigation ditches, that carried water, primarily from rivers, to fields for irrigation, were rarely used as sources of drinking water for humans; hence, they were not taken into consideration in the dose assessment. Contamination of water in acequias as a source for livestock was also not quantified for reasons that the surface area for collecting fallout would be extremely small compared to lakes and rivers.

The contamination of drinking water from cisterns, wells, public network, and rivers was estimated as follows.

Cisterns. The normalized time-integrated concentrations in drinking water from cisterns were obtained as:

$$
\frac{IC_{cist}(Z.L)}{A_{gd}\left(Z, L, \frac{R}{V}, TOA\right)} = P\left(R(L)|A_{gd}\right)\; \frac{S_{roof}}{V+\left(R(L)\;S_{roof}\right)}\; \frac{e^{-\lambda_e\;TD}}{\lambda_e} \qquad (25)
$$

where

S_{roof} = the area of the roof from which rainwater was collected, taken to be 10 m^2;

V is the volume of water in the cistern at the time of the test; V is assumed to correspond to an average monthly rainfall of 30 mm (= L m^{-2}), so that $V = S_{roof}\,x\,30 = 300$ L;

$P(R(L)/A_{gd}) = 1$ if rainfall occurred during the day of fallout in precinct L;

$P(R(L)/A_{gd}) = 0$ if rainfall did not occur during the day of fallout. It was assumed that the rain $R(L)$ that fell in the precinct during the day of fallout transferred to the cistern the activity deposited on the roof. The volume of water available immediately after rainfall at *TOA* was, therefore, $V + (R(L) \times S_{roof})$. It was also assumed that rainfall that occurred during the days before and after the day of fallout did not remove any of the activity deposited on the roof;

$\lambda_e = \lambda + \lambda_d$, in d^{-1}, where λ_d represents the rate of decrease of the concentration in the cistern water, assumed to correspond to a half-time of 15 d, due to the sedimentation of the activity on the bottom of the cistern and on the replenishment of the cistern with uncontaminated water. Because of this relatively short half-time, which was assumed to be applicable to all radionuclides, the cistern water was only contaminated during the first few months after the test; and

TD = the time delay between rainfall at *TOA* and the consumption of water, taken to be equal to 0.1 d.

Fig. 3. Map of rivers in New Mexico (derived from US Census).

Wells. The water originating from wells was unlikely to have been contaminated to a substantial degree by the fallout from Trinity. The time-integrated concentration of any radionuclide from Trinity in well water was taken to be equal to zero.

Public water networks. In the absence of measurements in New Mexico after the Trinity test, the estimation of the normalized time-integrated concentrations in tap water is very uncertain. For that reason, we derived an empirical relationship between the radionuclide concentration in tap and rainwater. Measurements made in French Polynesia after the nuclear tests carried out at Mururoa and Fangataufa showed that the β activities in tap water were about 15 to 20 times lower than in rainwater (Ministère 2006). In the

absence of information for New Mexico or for specific radionuclides, it was assumed that the time-integrated concentrations of any radionuclide from Trinity in tap water were 20 times lower than in rainwater. Rivers were assumed to be the main source of water for the public water supply. The calculation of the contamination of river water considered the probability that rainfall (occurring during a 30-min storm every day) happened during the passage of the radioactive cloud at *TOA*. Other assumptions made were: (1) the contamination of the river water was only due to wet deposition, and (2) the time-integrated concentration was obtained using a half-time of 15 d for the removal due to environmental loss processes.

Ingestion of leafy vegetables (lettuce, spinach, etc.)

The activity intakes by man from leafy vegetables, *LV*, resulted from the direct deposition of radionuclides from the cloud at TOA. The leafy vegetables were assumed to be ready to be harvested at the time of fallout deposition in 1945. The normalized time-integrated concentrations, in Bq d kg^{-1} per Bq m^{-2}, were expressed as:

$$\frac{IC_{LV}(Z,L)}{A_{veg}\left(Z,L,\frac{R}{V},TOA\right)} = \frac{CF(Z,LV)}{Y_{wet}(LV)\,\lambda_e(Z,LV)} \qquad (26)$$

where:

- the deposition, A_{veg}, in Bq m^{-2}, corresponds to the deposition on leafy vegetables;
- the culinary factor, *CF(Z, LV)*, has 2 components. (1) $CF_1(Z, LV)$, which is the decrease in concentration due to the culinary preparation, consisting in washing and removing the outer leaves for the leafy vegetables; according to Simmonds and Linsley (1982): $CF_1(Z, LV) = 0.2$ for Sr, Cs, and Pu, this value was used for all radionuclides; and (2) $CF_2(Z, LV)$, which is the decrease in concentration between harvesting and consumption. The values of $CF_2(Z, LV)$ were calculated accounting for the delay between harvesting and consumption to be equal to 1 d for urban precincts and 0.1 d for rural precincts, corresponding to the minimum delay time recommended in Table 81 of IAEA (2010) for urban precincts and to an even lower time for rural precincts. The rationale for selecting such low values is that the delay times in 1945, when refrigeration was not yet widespread, were likely to have been lower than those for more modern times as reported in IAEA (2010). The values of *CF(Z, LV)* were obtained as the products of $CF_1(Z, LV)$ and $CF_2(Z, LV)$;
- $Y_{wet}(LV)$ is the standing crop biomass expressed in terms of wet weight [kg (wet weight) m^{-2}]. Taking the water content of leafy vegetables to be 90% (IAEA 2010), the ratio of dry to wet weight is 10, so that $Y_{wet}(LV) = 3$ kg (wet weight) m^{-2};
- $\lambda_e = \lambda + \lambda_d$ where λ_d, in d^{-1}, represents the rate of decrease of the concentrations in leafy vegetables due to weathering processes, assumed to correspond to half-times of environmental removal of 10 d for stable iodine, 13 d for stable strontium, 14 d for stable cesium, and 15 d for all other elements (Thiessen and Hoffman 2018).

Ingestion of fruit vegetables (*FV*)

Fruit vegetables, *FV*, were assumed to be ready for harvest at the time of fallout deposition in 1945, and that they also continued to ripen during the following 90 d after *TOA*. Based on the results provided during the focus-group sessions and the key-informant interviews, the typical fruit vegetable consumed was cooked squash (Potischman et al. 2020). The normalized time-integrated concentrations were calculated as:

$$\frac{IC_{FV}(Z,L)}{A_{veg}\left(Z,L,\frac{R}{V},TOA\right)} = \frac{TF(Z,FV)\;\;CF(Z,FV)}{Y_{wet}(FV)\;\;\lambda_e(Z,FV)}, \qquad (27)$$

where:

- the deposition A_{veg} corresponds to the deposition on the leaves and on the fruit of the plant;
- the values of λ_e and of Y_{wet} are the same as those selected for the leafy vegetables;
- the transfer factor from deposition to fruit (*TF*) is assumed to be the sum of *TF1* and *TF2*: (1) for fruit vegetables ready to be harvested immediately after *TOA*, *TF1* corresponds to direct deposition on the fruit and is equal to 1 since translocation does not have to be taken into account; (2) for fruit vegetables that had not ripened yet at *TOA*, the translocation factor *TF2* from leaves to fruit must be used. For this pathway, *TF2* is expressed as the fraction of deposition on the leaves (per unit area of ground) that is transferred to the fruit. Selected values of the probability distribution of *TF2* for the elements considered in this study are presented in Table 11. In the calculations for the translocation of the specific radionuclides considered in this study, the time taken for the contamination deposited on the leaves to be transferred to the fruit was taken to be equal to 10 d. These translocation factors, which depend on the plant characteristics, the stage of plant growth, and the characteristics of the deposition (wet or dry), have considerable uncertainty (Thiessen and Hoffman 2018); and
- *CF(Z, FV)* is the product of *CF1* and *CF2*. The values of *CF1* were subjectively estimated to be 0.7 for all radionuclides. The values of $CF_2(Z, FV)$ were calculated accounting for the delay between harvesting and consumption to be equal to 2 d for urban precincts and 0.2 d for rural precincts, corresponding to the minimum delay time recommended in IAEA (2010) for urban precincts and to an even lower time for rural precincts. The rationale for selecting such low values is that the delay times in 1945 were

likely to have been smaller than those for more modern times reported in IAEA (2010).

Ingestion of fruit and berries (*FB*)

Fruit and berries, *FB*, were assumed to be ready to be harvested at the time of fallout deposition, *TOA*. Based on the results provided from the focus groups and the key informant interviews, the fruits consisted mainly of apples and different types of berries (Potischman et al. 2020). The normalized time-integrated concentrations were calculated using equation 27 and appropriate values for its parameters, the main difference being in the estimation of *CF1*. Reported values for the reduction in concentrations due to washing berries are 0.76 for Cs and 0.64 for Sr (Carini 1999). For the purposes of this study, a value of 0.7 was selected for *CF1* and was assumed to be the same for all radionuclides.

Ingestion of fresh cow's milk, *CM*

In order to estimate the time-integrated concentrations in fresh cow's milk, the intake of radionuclides by the cow, the transfer from feed to milk, and the origin and amount of milk consumed in the precinct need to be taken into consideration as follows:

- Estimation of the intake of radionuclides by the cow. Milk cows are generally fed hay and grains but were assumed to be highly dependent in New Mexico in 1945 on pasture grass during the pasture season. Because of the importance of pasture grass to the radionuclide intake of dairy cows, we assumed pasture grass to be the primary source of contamination and that the other pathways of intake, such as inhalation and soil consumption, were negligible. The contamination of pasture grass was due to direct deposition at *TOA* and decreased with time because of radioactive decay and environmental removal processes, with half-times of up to 15 d. The consumption of pasture grass *PG* by cows in New Mexico, was taken to be different in irrigated areas, where there was a heavy dependence on hay for most of the year, rather than fresh pasture, and in dry land areas, where most of the cow's intake was from pasture. The consumption of pasture grass was assumed to be 2.5 kg d^{-1} (dry) (NCI 1997) in irrigated areas and 5 kg d^{-1} (dry) in dry land areas. The irrigated areas were assumed to be the precincts with rivers and the dry lands areas in the other precincts, without rivers (Fig. 3). Under these assumptions, the radionuclide intake by dairy cows, *ICOW*, in Bq, due to direct deposition on pasture grass only occurred in 1945 during a few months after the explosion and was calculated as:

$$ICOW(Z,L) = A_{veg}(Z,L,R/V,TOA)\ x\ \frac{PG(L)}{Y_{wet}(L)\,\lambda_e(Z)} \qquad (28)$$

- Estimation of the transfer from feed to milk. The time-integrated concentrations in cow's milk, IC_{CM} in Bq d L^{-1}, are estimated using the transfer factor from animal feed-to-milk, usually designated as F_m. They are calculated as:

$$IC_{CM}\ (Z,L) = ICOW\ (Z,L)\ x\ F_m(element)\ x\ HL(Z). \qquad (29)$$

Selected values for the central estimates of F_m, in d L^{-1}, for the stable *elements* corresponding to the radionuclides under consideration are presented in Table 12. In order to obtain the F_m value for a specific radionuclide, *Z*, the F_m value for the corresponding *element* was multiplied by a factor $HL(Z) = T_r/(T_r + T_b)$, where T_r, in days, is the radioactive half-life of radionuclide *Z* and T_b is the biological half-time of the element in the cow, taken to be equal to 2 d (Thiessen and Hoffman 2018); and

- Estimation of the origin and amount of milk consumed in the precinct. Because the number of milk cows was not sufficient in some of the counties in New Mexico to provide enough milk for the population of the county, it was necessary to estimate the origin and amount of milk imported from other counties. This was done based on information on the milk production, use, and consumption, which was estimated on a county basis for the 1950s (NCI 1997). In that analysis, the state of New Mexico was divided into five relatively homogeneous milk regions, *MR*, and the distribution of milk was first considered to occur within the same milk region (Fig. 4). As shown in Table 13, *MR* 351 was the only region with an excess of milk. The other milk regions received some milk from *MR* 351 and some from other states (Arizona, Colorado, Kansas, and Texas). The estimated annual volumes of milk consumed in each *MR* in the 1940s, *VTOT* in kL, are given in

Table 11. Element-dependent values of the translocation factor from leaves to fruit.

Element	Fe, Zr, Nb, Sb, Ce, Pr	Co	Sr, Ba	Ru	Sb	Te, I, Cs	Nd	Pu, U
Distribution type				Log-uniform				
Minimum (%)	0.1	0.3	0.01	0.01	0.1	0.5	0.1	0.0001
Maximum (%)	10	30	10	1	10	50	10	0.01
Average (%)	1	3	0.3	0.1	1	5	1	0.001

Table 14, along with their origin, distributed into three categories: local (from the same milk region, *VL*), imported from *MR* 351 in New Mexico (*VNM*), and imported from other states (*VOS*). The imported volumes of milk were distributed in the counties of the milk region *MR* according to their needs. Prior to that operation, a distribution within the *MR* was carried out in order to provide enough milk to the counties with small deficits to be in, or closer to, equilibrium. It was not necessary to transfer milk from one county to another in *MR* 352, 353, and 354 because all counties of those *MR*s were in deficit.

Estimation of the time-integrated concentrations in milk

The time-integrated concentration of radionuclide *Z* in the milk *produced* in precinct *L, $ICP_{CM}(Z, L)$* in Bq d L^{-1}, was expressed as:

$$ICP_{CM}\,(Z,L) = ICOW\,(Z,L)\;x\;F_m(Z). \qquad (30)$$

Different procedures were used for the calculation of the time-integrated concentrations in *consumed* milk in the precinct according to whether: (1) there was excess milk in the county where the precinct is located, (2) there was a deficit of milk in the county but it was met with a supply from another county in the same milk region, or (3) the deficit of milk in the county was met with supplies from other milk regions of New Mexico and regions from other states.

Precincts in category 1 (*MC1*): excess of milk in the county. Assuming a delay of 2 d between production and consumption, the time-integrated concentration, $IC_{CM,MC1}$ in Bq d L^{-1}, of radionuclide *Z* in the milk *consumed* in precinct *L1* located in a county *CTY1* with excess milk was obtained as:

$$IC_{CM,MC1}(Z,L1) = ICP_{CM}\,(\mathrm{Z},L1)\;x\;\mathrm{e}^{-\lambda(Z)\;x\;2}. \qquad (31)$$

In the absence of information on the production of cows' milk at the level of the precinct, it was assumed that the

Table 12. Central estimates of the transfer factor from feed-to-milk for cows (d L^{-1}) for the stable elements corresponding to the radionuclides considered in the study.

Element	F_m (d L^{-1})	Element	F_m (d L^{-1})	Element	F_m (d L^{-1})
Fe	3.7×10^{-5}	Tc	0	Cs	4.9×10^{-3}
Co	3.2×10^{-4}	Ru	9.4×10^{-6}	Ba	1.8×10^{-4}
Cu	1.8×10^{-4}	Rh	1.0×10^{-4}	La	1.0×10^{-4}
As	1.4×10^{-4}	Ag	0	Ce	1.5×10^{-5}
Br	0	Pd	1.0×10^{-4}	Pr	1.0×10^{-4}
Rb	0	Cd	2.6×10^{-4}	Nd	1.0×10^{-4}
Sr	1.3×10^{-3}	In	0	Pm	1.0×10^{-4}
Y	1.0×10^{-4}	Sn	1.0×10^{-4}	Sm	1.0×10^{-4}
Zr	3.6×10^{-6}	Sb	3.8×10^{-5}	U	2.5×10^{-3}
Nb	4.1×10^{-7}	Te	3.2×10^{-4}	Np	1.0×10^{-4}
Mo	1.2×10^{-3}	I	6.0×10^{-3}	Pu	3.6×10^{-5}

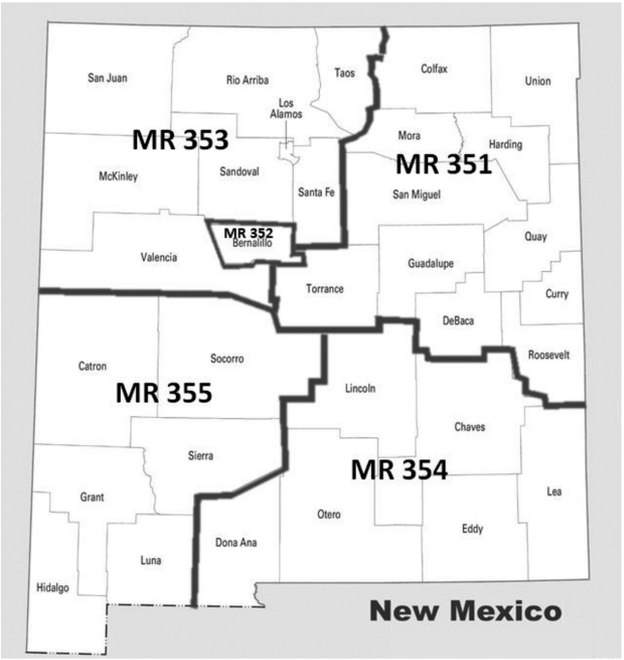

Fig. 4. Map of milk regions (derived from NCI 1997).

average time-integrated concentration of radionuclide *Z* in the milk *produced* in county *CTY1* where *L1* is located was equal to the mean of the values obtained for all precincts of the county:

$$ICP_{CM,AV}\,(Z,CTY1) = [\textstyle\sum ICP_{CM}\,(Z,L1)]/N(L1) \qquad (32)$$

where *N* is the number of precincts in the county.

Precincts in category 2 (*MC2*): deficit of milk in the county, met with supply from the same *MR*. The volumes of milk transferred from one county to another were denoted as *VTR*, Specifically, in *MR* 351, some of the excess milk from Quay county (1,092 kL) was transferred to Guadalupe (*VTR* = 181 kL), Mora (*VTR* = 58 kL), and San Miguel counties (*VTR* = 853 kL), so that the excess volume of milk in Quay county was reduced to 575 kL. In *MR* 355, excess milk from Catron county (92 kL) was transferred to Socorro (*VTR* = 70 kL) and to Grant counties (*VTR* = 22 kL), and excess milk from Sierra (163 kL) was transferred to Hidalgo (*VTR* = 118 kL) and to Luna counties (*VTR* = 45 kL). The volumes transferred were sufficient to cover the consumption of milk in Guadalupe, Mora, San Miguel, Hidalgo, and Sierra counties, but served only to reduce the deficit in Grant and Luna counties (Table 13).

The time-integrated concentration of radionuclide *Z* in the milk *produced,* or more exactly, available for consumption in a precinct *L2* of a county *CTY2* with a deficit milk *VTR* that was provided by another county with excess milk *CTY1* from the same milk region (either *MR* 351 or *MR* 355) has two components: (1) the milk for fluid use, *TMFU*, available in *CTY2*;

Table 13. Estimated annual production, distribution, and consumption of fresh cows' milk in New Mexico (based on NCI 1997).

County name	Milk region	Production kL	TMFU[a] kL	Consumption kL	EXC[b] kL	EXC2[c] kL
COLFAX	351	3,192	1,897	1,697	200	200
CURRY	351	6,400	3,805	2,991	814	814
DE BACA	351	957	569	357	212	212
GUADALUPE	351	852	506	687	−181	0
HARDING	351	1,060	630	277	353	353
MORA	351	1,297	771	829	−58	0
QUAY	351	5,243	3,117	1,450	1,667	575
ROOSEVELT	351	16,134	9,592	1,786	7,806	7,806
SAN MIGUEL	351	3,210	1,908	2,761	−853	0
TORRANCE	351	3,258	1,936	806	1,130	1,130
UNION	351	4,970	2,955	746	2,209	2,209
BERNALILLO	352	6,082	5,590	21,374	−15,784	−15,784
MCKINLEY	353	134	123	3,459	−3,336	−3,336
RIO ARRIBA	353	1,886	1,733	2,700	−967	−967
SANDOVAL	353	612	563	2,710	−2,147	−2,147
SAN JUAN	353	3,594	3,303	3,632	−329	−329
SANTA FE	353	1,017	934	4,495	−3,561	−3,561
TAOS	353	2,028	1,205	1,821	−616	−616
VALENCIA	353	5,000	2,972	3,234	−262	−262
CHAVES	354	2,748	2,525	5,239	−2,714	−2,714
DONA ANA	354	3,101	2,849	5,280	−2,431	−2,431
EDDY	354	4,205	3,864	4,922	−1,058	−1,058
LEA	354	3,643	3,348	4,420	−1,072	−1,072
LINCOLN	354	1,258	748	826	−78	−78
OTERO	354	1,403	1,289	2,659	−1,370	−1,370
CATRON	355	745	443	351	92	0
GRANT	355	1,279	1,175	2,233	−1,058	−1,036
HIDALGO	355	728	433	551	−118	0
LUNA	355	825	758	1,008	−250	−205
SIERRA	355	1,537	913	750	163	0
SOCORRO	355	1,102	1,012	1,082	−70	0

[a]TMFU = total milk annually available for fluid use (kL).
[b]EXC = excess or deficit of milk (kL), prior to distribution.
[c]EXC2 = excess or deficit of milk (kL), after transfer from a county in the same milk region.

and (2) the deficit, *VTR(CTY1, CTY2)*, covered in its entirety, with the exception of Grant and Luna counties, by the transfer of milk from *CTY1*. In the absence of information on the distribution of *TMFU* and of *VTR* at the precinct level, it was assumed that the ratio for *CTY2* of *TMFU(CTY2/[(TMFU(CTY2) + VTR(CTY1, CTY2)]* had the same value for each precinct *L2*:

$$ICP_{CM,MC2}(Z,L2) = [(ICP_{CM}(Z,L2)\ x\ TMFU(CTY2)) + (ICP_{CM},AV(Z,CTY1)\ x\ VTR(CTY1,CTY2)))/[(TMFU(CTY2) + VTR(CTY1,CTY2)]. \quad (33)$$

Assuming a delay of 3 d between availability and consumption, the time-integrated concentration, $IC_{CM,MC2}$ in Bq d L^{-1}, of radionuclide *Z* in the milk *consumed* in precinct *L2* located in a county *CTY2* with deficit milk supplied by

Table 14. Origin and amount of consumed milk in each milk region of New Mexico (kL).

Milk region MR	Origin and annual amount of consumed milk (kL) VL: from same MR	VNM: imported from MR 351	VOS: imported from other States	VTOT: total
351	14,599	0	0	14,599
352	5,590	9,168	6,706	21,464
353	10,833	1,834	9,119	21,786
354	14,623	1,523	7,197	23,343
355	4,734	458	782	5,974

excess milk from another county, *CTY1*, from the same milk region was obtained as:

$$IC_{CM,MC2}(Z,L2) = ICP_{CM,MC2}(Z,L2)\ x\ e^{-\lambda(Z)\ x\ 3}. \quad (34)$$

For Grant and Luna counties, additional amounts of milk had to be imported from other areas in order to cover in its entirety the consumption of milk in those counties.

Precincts in category 3: deficit of milk in the county, met with supply from milk region 351 of New Mexico and from other states. All counties (and precincts) are in category 3 in *MR* 352, 353, and 354, as well as Grant and Luna counties in *MR* 355.

The time-integrated concentration, $ICP_{CM,3}$ in Bq d L^{-1}, of radionuclide *Z* in the milk *produced,* or more exactly, available for consumption in a precinct *L3* of a county *CTY3* with a residual deficit of milk (see last column of Table 13) has three components: (1) the milk for fluid use, *TMFU*, in kL, available in *CTY3*; (2) the volume of milk, *VNM(MR351, CTY3)*, transferred from *MR* 351; and (3) the volume of milk, *VOS*, transferred from other states. As it was assumed that the milk from other states was not contaminated by fallout from Trinity, the third component was not considered. Also, in the absence of information on the distribution of *TMFU* at the precinct level, it was assumed that the ratio for *CTY3* of *TMFU(CTY3)/CONS(CTY3)* had the same value for each precinct *L3*:

$$ICP_{CM,MC3}(Z,L3) = [(ICP_{CM}\ (Z,L3)\ x\ TMFU(CTY3)) + (ICP_{CM,AV}\ (Z,MR351)\ x\ VNM\ (MR351,CTY3))]/CONS(CTY3) \quad (35)$$

where the value of *VNM* for the milk region (Table 14) was apportioned to its counties *CTY3* with milk deficits according to the volumes of milk consumed, *CONS(CTY3)*, and the time-integrated concentration, $ICP_{CM,AV}$ in Bq d L^{-1}, of radionuclide *Z* in the milk *produced* in *MR* 351 was obtained as:

$$ICP_{CM,AV}\ ((Z,MR351) = \left[\sum ICP_{CM,AV}\ (Z,CTY4)\ x\ EXC2(CTY4)\right]/\sum EXC2(CTY4) \quad (36)$$

where *CTY4* is a county in *MR* 351 and *EXC2* is its excess of milk after distribution in the milk region (Table 13).

Assuming a delay of 4 d between availability and consumption, the time-integrated concentration, $IC_{CM,MC3}$ in Bq d L^{-1}, of radionuclide *Z* in the milk *consumed* in precinct *L3* located in a county *CTY3* with deficit milk supplied by excess milk from MR351 and from other states was obtained as:

$$IC_{CM,MC3}(Z,L3) = ICP_{CM,MC3}(Z,L3)\ x\ e^{-\lambda(Z)x\ 4}. \quad (37)$$

Exceptions are Grant and Luna counties, which are the only counties with milk categories 2 and 3. The time-integrated concentration of radionuclide *Z* in the milk *consumed* in precinct *L3* located in Grant or in Luna county was obtained as:

$$IC_{CM,MC3}(Z,L3) = \{\left[ICP_{CM,MC2}(Z,L3)\,x\,(TMFU(CTY3) + VTR(CTY1,CTY3))\,x\,e^{-\lambda(Z)x3}\right] + \left[(ICP_{CM,AV}\,(Z,MR351)\,x\,VNM\,(MR351,CTY3))\,x\,e^{-\lambda(Z)x4}\right]\}/CONS(CTY3). \quad (38)$$

Ingestion of cow cheese, *CC*

The normalized time-integrated concentrations in soft cow cheese were derived from the normalized time-integrated concentrations in cow's milk of local origin (same precinct), considering the values of the culinary factor, *CF (Z, CC)*:

$$\frac{IC_{CC}(Z,L)}{A_{veg}(Z,L)} = \frac{ICP_{CM}(Z.L)}{IC_{veg}(Z,L)}\ CF(Z,CC) \quad (39)$$

where *CF (Z, CC)* has two components, such that $CF = CF_1 \times CF_2$:

- the culinary preparation, CF_1, which involves both the processing efficiency (weight of cheese per weight of milk) and the retention of the radionuclide in the cheese compared with milk. The value of CF_1 is obtained as the ratio of the values for the retention and for the processing efficiency. From limited information, CF_1 is about 0.1/0.12 = 0.8 for most elements but could be as high as 0.7 / 0.12 = 5.8 for strontium. For the purposes of this study, the proposed values of *CF1* are 5 for isotopes of strontium and 1 for all other radionuclides; and
- CF_2, which represents the reduction in concentration due to radioactive decay during the time delay, estimated to be 3 d, between the production of the soft cow cheese and its consumption.

Ingestion of beef (*BF*), mutton (*MT*), and pork (*PK*)

The normalized time-integrated concentrations in beef, mutton, and pork, in Bq d kg^{-1}, were estimated in the same manner. Taking, for example, beef, the following equation was used:

$$\frac{IC_{BF}(Z.L)}{A_{veg}\left(Z,L,\frac{R}{V},TOA\right)} = \frac{PG_{BF}(L)}{Y_{wet}(L)\,\lambda_e(Z)}\ F_f(element,BF)\ \frac{T_r(Z)}{T_r(Z)+T_b(BF)}\ CF_{BF}(Z) \quad (40)$$

where:

- $PG_{BF}(L)$ is the pasture-grass intake of beef cattle, estimated to be 10 kg (dry mass) d^{-1}; the corresponding values for sheep and swine were assessed to be 1.5 and 0.7 kg (dry mass) d^{-1}, respectively;
- F_f *(element, BF)* is the feed-to-meat transfer coefficient for beef cattle (d kg^{-1}) for the element. The selected values for F_f(*element*), as well as their probability distributions, are presented in Table 15 for beef, mutton, and pork (Thiessen and Hoffman 2018);

- $\frac{T_r(Z)}{T_r(Z)+T_b(BF)}$ is the expression which, when multiplied by F_f (*element, BF*), provides the value of F_f *(Z, BF)*, *Z* being a radioactive isotope of the element considered. The parameter $T_b(BF)$ represents the biological half-time of the radionuclide in meat (muscle tissue). A value of 30 d was selected for all radionuclides and for beef, mutton, or pork; and
- The culinary factor CF_{BF} represents essentially the loss of activity due to the delay between *TOA* and the time of slaughter. It was assumed that all slaughter of beef cattle, sheep, and swine occurred in the fall or winter; that is, at least 60 d after *TOA*. The values of CF_{BF} were calculated assuming radioactive decay during a period of 30 d between *TOA* and slaughter and an additional 1 d between slaughter and consumption.

Ingestion of mothers' milk (MM)

The time-integrated concentrations in mothers' milk, IC_{MM} in Bq d L^{-1}, were obtained by means of a different procedure:

$$IC_{MM}(Z,L) = IMOT(Z,L)\, F_{MM}(element)\, \frac{T_r(Z)}{T_r(Z)+T_b(MM)} \qquad (41)$$

where

- *IMOT(Z, L)* is the sum of the activity intakes, in Bq, by the mother, from drinking water and from the consumption of all foodstuffs;
- F_{MM} *(element)* is the intake-to-mothers' milk transfer coefficient (d L^{-1}) for the element. The selected values for F_{MM} *(element)* are presented in Table 16 (ICRP 2004; Simon et al. 2010b); and
- $\frac{T_r(Z)}{T_r(Z)+T_b(MM)}$ is the expression which, when multiplied by F_{MM} *(element)*, provides the value of $F_{MM}(Z)$, Z being a radioactive isotope of the element considered. In this equation, $T_r(Z)$ is the radioactive half-life (d) of radionuclide Z. The parameter $T_b(MM)$ represents the biological half-time of the radionuclide in mothers' milk. A value of 2 d was selected for all radionuclides.

Normalized intakes by inhalation and ingestion (Q_{pw}/IC_{pw})

- The normalized intakes, Q_{pw}/IC_{pw}, consist of the breathing rates for the inhalation pathways and of the consumption rates of water and foodstuffs for the ingestion pathways.

Table 15. Selected log-triangular probability distributions for the feed-to-meat transfer coefficients, in d kg^{-1}, for beef, mutton,[a] and pork[a] (Thiessen and Hoffman 2018).

	Beef			Mutton			Pork		
	Mode	Min.	Max.	Mode	Min.	Max.	Mode	Min.	Max.
Fe	1.4×10^{-2}	4.7×10^{-3}	4.2×10^{-2}				3.0×10^{-3}	4.0×10^{-4}	3.0×10^{-2}
Co	4.3×10^{-4}	1.3×10^{-4}	1.3×10^{-3}	1.2×10^{-2}	1.2×10^{-3}	1.2×10^{-1}			
As	2.0×10^{-2}	2.0×10^{-3}	2.0×10^{-1}						
Sr	1.3×10^{-3}	2×10^{-4}	9.2×10^{-3}	1.5×10^{-3}	3.0×10^{-4}	4.0×10^{-3}	2.5×10^{-3}	5.0×10^{-4}	8.0×10^{-3}
Y	7.5×10^{-4}	7.5×10^{-5}	7.5×10^{-3}						
Zr	1.2×10^{-6}	1.2×10^{-7}	1.2×10^{-5}						
Nb	2.6×10^{-7}	2.6×10^{-8}	2.6×10^{-6}						
Mo	1.0×10^{-3}	1.0×10^{-4}	1.0×10^{-2}						
Ru	3.3×10^{-3}	1.3×10^{-3}	1.0×10^{-2}	2.1×10^{-3}	2.1×10^{-4}	2.1×10^{-2}	3.0×10^{-3}	3.0×10^{-4}	3.0×10^{-2}
Rh	1.0×10^{-2}	1.0×10^{-3}	1.0×10^{-1}						
Cd	5.8. x.10^{-3}	1.5×10^{-4}	6.0×10^{-2}	1.2×10^{-3}	1.2×10^{-4}	1.2×10^{-2}			
Sn	1.0×10^{-2}	1.0×10^{-3}	1.0×10^{-1}						
Sb	1.2×10^{-3}	1.2×10^{-4}	1.2×10^{-2}						
Te	7.0×10^{-3}	7.0×10^{-4}	7.0×10^{-2}						
I	6.7×10^{-3}	2.0×10^{-3}	3.8×10^{-2}	3.0×10^{-2}	3.0×10^{-3}	3.0×10^{-1}	4.1×10^{-2}	4.1×10^{-3}	4.1×10^{-1}
Cs	2.2×10^{-2}	4.7×10^{-4}	9.6×10^{-2}	1.9×10^{-1}	5.3×10^{-2}	1.3×10^{0}	2.0×10^{-1}	7.0×10^{-2}	6.0×10^{-1}
Ba	1.4×10^{-4}	1.4×10^{-5}	1.4×10^{-3}						
La	1.3×10^{-4}	1.3×10^{-5}	1.3×10^{-3}						
Ce	2.0×10^{-2}	2.0×10^{-3}	2.0×10^{-1}	2.5×10^{-4}	2.5×10^{-5}	2.5×10^{-3}			
Pr	1.0×10^{-3}	1.0×10^{-4}	1.0×10^{-2}						
Nd	2.0×10^{-3}	2.0×10^{-4}	2.0×10^{-2}						
Pm	1.0×10^{-3}	1.0×10^{-4}	1.0×10^{-2}						
Sm	1.5×10^{-3}	1.5×10^{-4}	1.5×10^{-2}						
U	3.9×10^{-4}	1.3×10^{-4}	1.2×10^{-3}				4.4×10^{-2}	4.4×10^{-3}	4.4×10^{-1}
Np	1.0×10^{-3}	1.0×10^{-4}	1.0×10^{-2}						
Pu	1.1×10^{-6}	8.8×10^{-8}	3.0×10^{-4}	5.3×10^{-5}	5.3×10^{-6}	5.3×10^{-4}			

[a] Beef was used as a surrogate when specific transfer coefficients were not available.

Breathing rates

- The breathing rates *BR* as a function of age were taken from ICRP Publication 66 (ICRP 1994). The selected values, which correspond to light exercise, are averaged over males and females and are assumed to be the same for Hispanics, Whites, Native Americans, and African Americans, depending on the age of the representative individual under consideration: 0.19 m^3 h^{-1} for infants under 1 y of age, 0.35 m^3 h^{-1} for 1- to 2-y-old infants, 0.57 m^3 h^{-1} for 3- to 7-y-old children, 1.25 m^3 h^{-1} for 8- to 12-y-old children, 1.40 m^3 h^{-1} for 13- to 17-y-old teenagers, and 1.38 m^3 h^{-1} for adults.

Consumption rates of drinking water and foodstuffs

- The consumption rates of drinking water, in L d^{-1}, and of foodstuffs, in kg d^{-1}, considered in the dose assessment are presented in Table 17. For all foodstuffs other than mother's milk, the consumption rates *CR* for Hispanics, Whites, and Native Americans, which vary according to data set and to age group, were derived from information collected from the focus groups and interviews with key informants that were conducted in various locations of New Mexico (Potischman et al. 2020). For reasons of necessity, that information was collected for age groups that are different from those used in the dose assessment. The values presented in Table 17 were interpolated from the collected data using the assumption that the annual consumption rates do not vary from year to year in the same age group.
- The consumption rates of drinking water and of mother's milk were derived from literature values. The total consumption rate of water (drinking water, other beverages, foodstuffs) was taken to be 2.2 L d^{-1} among adults, as recommended in ICRP Publication 89 (ICRP 2002). The consumption rates of only drinking water were assumed to be equal to the total consumption of water minus the consumption of cow's milk. The variation with age of the total consumption rate of water was assumed to be proportional to the urine excretion rate, also given in ICRP Publication 89. The rounded values that were obtained for the consumption of drinking water vary with age but are independent of the data set (Table 17).
- The consumption rates of mother's milk, presented in Table 17, were taken from ICRP Publication 95 (ICRP 2004). Based on the information provided by Potischman et al. (2020), the consumption of mother's milk was assumed to occur during the entire first year of age. It was also assumed that no other foodstuff was consumed by infants <1 y of age.

Table 16. Selected values of the fraction transferred to the infant in breast milk following maternal intake, in d L^{-1}(ICRP 2004; Simon et al. 2010b).

Element	F_{MM}	Element	F_{MM}	Element	F_{MM}
Fe	2.2×10^{-3}	Tc	1.0×10^{-1}	Cs	1.2×10^{-1}
Co	3.5×10^{-2}	Ru	2.2×10^{-3}	Ba	5.8×10^{-3}
Cu	4.1×10^{-2}	Rh	3.4×10^{-3}	La	2.3×10^{-3}
As	4.0×10^{-2}	Ag	1.1×10^{-2}	Ce	2.1×10^{-5}
Br	8.5×10^{-2}	Pd	2.8×10^{-4}	Pr	2.3×10^{-5}
Rb	8.5×10^{-2}	Cd	3.3×10^{-3}	Nd	2.3×10^{-5}
Sr	6.1×10^{-2}	In	1.2×10^{-3}	Pm	2.3×10^{-5}
Y	4.1×10^{-6}	Sn	1.2×10^{-3}	Sm	2.3×10^{-5}
Zr	4.7×10^{-4}	Sb	4.7×10^{-3}	U	9.7×10^{-4}
Nb	2.8×10^{-4}	Te	2.9×10^{-3}	Np	4.1×10^{-5}
Mo	1.2×10^{-2}	I	3.3×10^{-1}	Pu	2.4×10^{-5}

Doses per unit intake (D_{pw}/Q_{pw})

- The absorbed doses per unit intake, also called dose conversion factors, to lung, thyroid, active marrow, stomach and colon, were estimated for the 63 radionuclides considered in the dose assessment, for intake via inhalation and ingestion, and for all ICRP post-natal age groups, namely newborn, 1–2 y, 3–7 y, 8–12 y, 13–17 y, and adults. In addition, specific consideration was given to the absorbed doses received in utero per unit intake by the mother.
- In order to estimate the conversion factors from intake to absorbed dose delivered during the first year after intake, extensive use was made of ICRP publications (ICRP 1989, 1993, 1995a and b, 2001, 2004) in which 50-y equivalent doses per unit intake are provided for the most important radionuclides. The selected values for the class of solubility in lung and for the gastro-intestinal fractions were based on a literature review (Ibrahim et al. 2010). For all 54 radionuclides with physical half-lives shorter than 3 mo, the doses per unit intake that are received during the first year following the test are approximately equal to the 50-y dose conversion factors. However, for the nine radionuclides with half-lives longer than 9 mo, only a fraction of the 50-y doses was delivered during the first year following the test. For these radionuclides, calculations were made of the first-year doses using specialized software consistent with the ICRP publications. For ^{239}Pu and ^{240}Pu, which are α-emitters, the low-LET and the high-LET components of the equivalent dose coefficients are provided separately in the software that was used. For the purposes of this study, the equivalent dose coefficients due to the high-LET component were divided by 20 (which is the W_R value for α particles) and added to the equivalent dose coefficients due to the low-LET component (for which the W_R value is equal to 1) in order to obtain the numerical values of the absorbed doses per unit intake, expressed in mGy Bq^{-1}.
- With respect to the absorbed doses received in utero per unit intake by the mother, use was made of specialized software,[7] consistent with the results presented in ICRP

Table 17. Estimation of the consumption rate (kg d^{-1} or L d^{-1}) according to age group and data set.

		Consumption rate (kg d^{-1} or L d^{-1})					
Foodstuff	Age, y	A	B	C	D	E	F
Mothers' milk	0 – 1	0.8	0.8	0.8	0.8	0.8	0.8
Drinking water	0 – 1	0.5	0.5	0.5	0.5	0.5	0.5
	1 – 2	0.4	0.4	0.4	0.4	0.4	0.4
	3 – 7	0.5	0.5	0.5	0.5	0.5	0.5
	8 – 12	0.7	0.7	0.7	0.7	0.7	0.7
	13 – 17	1.5	1.5	1.5	1.5	1.5	1.5
	Adult	1.9	1.9	1.9	1.9	1.9	1.9
Leafy vegetables	1 – 2	0.052	0.013	0.013	0.031	0.045	0.039
	3 – 7	0.094	0.021	0.021	0.066	0.061	0.068
	8 – 12	0.16	0.036	0.036	0.095	0.091	0.12
	13 – 17	0.23	0.086	0.086	0.13	0.15	0.21
	Adult	0.26	0.134	0.14	0.16	0.19	0.28
Fruit vegetables	1 – 2	0.045	0.011	0.011	0.027	0.039	0.044
	3 – 7	0.031	0.007	0.006	0.020	0.023	0.027
	8 – 12	0.031	0.007	0.006	0.018	0.018	0.023
	13 – 17	0.049	0.018	0.018	0.027	0.032	0.044
	Adult	0.057	0.030	0.030	0.036	0.042	0.060
Fruit and berries	1 – 2	0.028	0	0.55	0.028	0.005	0.11
	3 – 7	0.038	0	0.65	0.038	0.006	0.15
	8 – 12	0.057	0	0.85	0.057	0.011	0.19
	13 – 17	0.062	0	0.93	0.062	0.016	0.24
	Adult	0.041	0	0.77	0.041	0.020	0.28
Cow's milk	1 – 2	0.27	0.25	0.12	0.54	0.118	0.28
	3 – 7	0.48	0.38	0.15	0.53	0.189	0.33
	8 – 12	0.65	0.50	0.18	0.72	0.142	0.49
	13 – 17	0.65	0.39	0.19	0.84	0	0.53
	Adult	0.59	0.18	0.18	0.61	0	0.39
Cow's cheese	1 – 2	0.037	0.037	0	0	0	0
	3 – 7	0.044	0.044	0.008	0	0	0.004
	8 – 12	0.049	0.049	0.016	0	0	0.009
	13 – 17	0.050	0.050	0.019	0	0	0.011
	Adult	0.050	0.050	0.015	0	0	0.012
Beef	1 – 2	0.040	0.018	0.038	0.042	0.001	0.003
	3 – 7	0.063	0.031	0.058	0.070	0.006	0.004
	8 – 12	0.13	0.045	0.082	0.134	0.010	0.007
	13 – 17	0.16	0.055	0.10	0.20	0.013	0.010
	Adult	0.077	0.056	0.11	0.20	0.015	0.009
Mutton / Pork	1 – 2	0.004	0	0.003	0.022	0	0.011
	3 – 7	0.005	0	0.005	0.035	0	0.019
	8 – 12	0.006	0.021	0.006	0.069	0	0.025
	13 – 17	0.008	0.053	0.008	0.14	0	0.025
	Adult	0.008	0.053	0.009	0.20	0	0.023

Publication 88 (ICRP 2001). The time of intake was assumed to occur during the fifteenth week of pregnancy,

Uncertainties

- The uncertainties in the estimated doses from internal irradiation were evaluated for each term of the right side of eqn (7), reproduced below, with the exception of $\dot{X}(12)$, which was covered in the section "Absorbed Doses From External Irradiation:"

$$D_{pw}(Z,L,I,m) = \dot{X}(12,\ L).\frac{A_{pw}\,(Z,L,TOA)}{\dot{X}\,(12,L)}\ .\frac{IC_{pw}\,(Z,L)}{A_{pw}(Z,L,TOA)}\ .\frac{Q_{pw}\,(Z,L,I)}{IC_{pw}\,(Z,L)}.\frac{D_{pw}(Z,I,m)}{Q_{pw}(Z,L,I)}. \quad (7)$$

Uncertainties in the normalized deposition densities [$A_{pw}/\dot{X}$ (12, L)]

The important parameters influencing the estimates of the normalized deposition densities are:

- $\left(\beta/\dot{X}\right)_{\frac{R}{V},12}$, which is the ratio of the beta activity deposited on the ground and of the exposure rate at H+12 h for a given value of *R/V*. These ratios were derived from the findings of Hicks (1985) for *R/V* = 0.5 and Beck (2009) for other values of *R/V*. The probability distributions around the best estimate values were subjectively estimated to be log-normal with a GSD of 1.1;
- $(Z/\beta)_{\frac{R}{V},12}$ is the ratio of the activity of radionuclide *Z* and of the beta activity deposited on the ground for a given value of *R/V*. These ratios were obtained from the same sources as those used for $\left[\beta/\dot{X}(12)\right]_{\frac{R}{V},12}$. The probability distributions around the best estimate values were subjectively estimated to be log-normal with a GSD of 1.2;
- $F_{gd}(Z,TOA)$ is the function describing the variation with time of the activity of radionuclide *Z* deposited on the ground, according to the laws of radioactive decay. Its uncertainty was taken to be negligible;
- $N_{50}(L)$ is the fraction of total beta activity that is on particles <50 μm at *TOA*. Its deterministic value is used to assign the best estimate of *R/V* in the precinct under consideration. Its probability distribution around its best estimate was subjectively assumed to be triangular and to depend on the value of *R/V*: TRI (0.5, 1, 2) for *R/V* = 3, TRI (0.6, 1, 1.5) for *R/V* = 2, TRI (0.7, 1, 1.4) for *R/V* = 1.5, TRI (0.8, 1, 1.2) for *R/V* = 1, and no uncertainty for *R/V* = 0.5;
- f_{dry} is the fraction of the activity attached to particles <50 μm that is deposited and initially retained by vegetation as a result from deposition via dry processes. Its probability distribution around its best estimate was subjectively assumed to be triangular: TRI (0.5, 1, 2);
- f_{wet} is the fraction of the activity attached to particles of all sizes that is deposited and initially retained by vegetation as a result of deposition via wet processes, i.e., rain. Given the fact that the occurrence of rain during the passage of the radioactive cloud had a very small probability, the uncertainty in the value of f_{wet} was not taken into consideration.

Uncertainties in the normalized time-integrated concentrations (IC_{pw}/A_{pw})

All inhalation and ingestion pathways are considered in turn.

- Inhalation during the passage of the cloud. For any radionuclide, *Z*, deposited in any precinct, *L*, the probability distribution of IC_{cd}/A_{gd}, in Bq s m^{-3} per Bq m^{-2}, around its best estimate was subjectively assumed to be triangular: TRI (0.7, 1, 1.5);
- Inhalation due to resuspended material. For any radionuclide, *Z*, deposited in any precinct, *L*, the probability distribution of IC_{res}/A_{gd}, in Bq d m^{-3} per Bq m^{-2}, around its best estimate was taken to be the same as that estimated in Maxwell and Anspaugh (2011) for $S_f(t)$, that is, uniform, U(0.1, 10);
- Ingestion of drinking water. The uncertainty in the normalized time-integrated concentrations in drinking water, IC_{wt}/A_{gd}, in Bq d L^{-1} per Bq m^{-2}, depends on the origin of drinking water (cistern or public network), on the characteristics of the cistern systems and of the rivers, on the properties of the radionuclides, and on the validity of the models used to calculate the water concentrations. For any radionuclide, *Z*, and any precinct, *L*, the probability distribution of IC_{wt}/A_{gd} around its best estimate was subjectively assumed to be censored log-uniform (0.1, 10);
- Ingestion of leafy vegetables. The uncertainty in the normalized time-integrated concentrations in leafy vegetables, IC_{LV}/A_{veg}, in Bq d kg^{-1} per Bq m^{-2}, depends mainly on the uncertainty in the culinary preparation component of the culinary factor. For any radionuclide, *Z*, and any precinct, *L*, the probability distribution of IC_{LV}/A_{veg} around its best estimate was subjectively assumed to be log-normal with a geometric standard deviation of 1.3;
- Ingestion of fruit vegetables. The uncertainty in the normalized time-integrated concentrations in fruit vegetables, IC_{FV}/A_{veg}, in Bq d kg^{-1} per Bq m^{-2}, depends mainly on the uncertainty in the transfer factor from leaves to fruit. For any radionuclide, *Z*, and any precinct, *L*, the probability distribution of IC_{FV}/A_{veg}, around its best estimate was subjectively assumed to be log-uniform with lower and upper bounds equal to 0.1 and 10 times the deterministic value, respectively;
- Ingestion of fruit and berries. The uncertainty in the normalized time-integrated concentrations in fruit and berries, IC_{FB}/A_{veg}, in Bq d kg^{-1} per Bq m^{-2}, depends mainly on the uncertainty in the application of the model to different types of berries and of fruit. For any radionuclide, *Z*, and any precinct, *L*, the probability distribution of IC_{FB}/A_{veg} around its best estimate was subjectively assumed to be log-normal with a geometric standard deviation of 1.3;
- Ingestion of fresh cows' milk. The uncertainty in the normalized time-integrated concentrations in cows' milk, IC_{CM}/A_{veg}, in Bq d L^{-1} per Bq m^{-2}, depends essentially on the transfer factor from feed to milk and on the origin of milk. Estimated values for any radionuclide, *Z,* are LN (2.0) for precincts in counties with category-1 milk (Catron, Colfax, Curry, De Baca, Harding, Quay, Roosevelt, Sierra, Torrance, Union); LN(3.0) for precincts in counties with category-2 milk (Guadalupe, Mora, San Miguel, Socorro, Grant, Hidalgo, Luna); and LN(4.0) for precincts in counties with category-3 milk (Bernalillo, Mckinley, Rio Arriba, Sandoval, San Juan, Santa Fe, Taos, Valencia, Chaves, Dona Ana, Eddy, Lea, Lincoln, Otero);

[7]Personal communication, K. Eckerman and D. Melo; October 2017.

- Ingestion of cow cheese. The uncertainty in the normalized time-integrated concentrations in cow cheese, IC_{CC}/A_{veg}, in Bq d kg^{-1} per Bq m^{-2}, depends on the uncertainties in ICP_{CM}/A_{veg} and in CF, as well as on the uncertainties in the transfer factor from feed to milk and in the origin of milk. For any radionuclide, Z, and any precinct, L, the probability distribution of IC_{CC}/A_{veg} around its best estimate was subjectively assumed to be log-normal with a geometric standard deviation of 2.3;
- Ingestion of meat (beef, mutton, and pork). The uncertainty in the normalized time-integrated concentrations in beef, mutton, and pork, IC_{BF}/A_{veg}, in Bq d kg^{-1} per Bq m^{-2}, depends mainly on the uncertainty in the transfer coefficient from feed to meat, F_f. For any radionuclide, Z, and any precinct, L, the probability distribution of IC_{BF}/A_{veg} around its best estimate was subjectively assumed to be log-triangular with upper and lower bounds equal to 10 times higher and lower than the best estimate, respectively; and
- Ingestion of mother's milk. The uncertainty in the time-integrated concentrations in mother's milk depends mainly on the uncertainties on the total intakes by the mother and on the transfer of the radionuclides from the intakes to breast milk. For any radionuclide, Z, and any precinct, L, the probability distribution of IC_{MM}/A_{pw} around its best estimate was subjectively assumed to be equal to the uncertainty in cows' milk of category 1, that is, log-normal with a geometric standard deviation of 2.0.

Uncertainties in breathing rates and consumption rates (*Q/IC*)

The probability distribution of the breathing rate, Q/IC in m^3 d^{-1}, was subjectively estimated to be distributed as TRI(0.5, 1, 2) around the best estimate for any age and data set, while the probability distribution of the consumption rate of any foodstuff was subjectively estimated to be log-normal with a GSD of 1.3 around the best estimate, also for all ages and data sets.

Uncertainties in doses per unit intake (*D/Q*)

The probability distribution of the dose per unit intake, D/Q in mGy Bq^{-1}, for a given radionuclide varies, among other factors, according to the mode of exposure (inhalation or ingestion), the organ/tissue under consideration, the characteristics of the population group (age and sex), the level of complexity of the biokinetics and dosimetry relevant to the considered radionuclide, and the quality of the underlying information. In this analysis, the elements were classified according to a subjective reliability index (low, medium, or high) and all radionuclides of the element were assumed to have the same reliability index for all age groups (Table 18).

The way in which the uncertainties in the individual parameters were combined to evaluate the uncertainties in the dose estimates is provided in Simon et al. (2020).

SUMMARY

The purpose of this document is to provide detailed information on the methods, models, and parameter values that were used in the assessment of the radiation doses that were received by New Mexico residents as the result of the detonation of the Trinity test (Simon et al. 2020). Three pathways of human exposure were included: (1) external irradiation, arising mainly from the radionuclides deposited on the ground, and, for a small part, from radionuclides in the passing cloud, (2) inhalation of radionuclide-contaminated air during the passage of the radioactive cloud and, thereafter, of radionuclides transferred (resuspended) from soil to air, and (3) ingestion of contaminated water and foodstuffs. To the extent possible, well established models and parameter values were adopted for the calculation of the doses resulting from those three pathways. Sixty-three radionuclides and five organs or tissues (thyroid, lung, active marrow, stomach, and colon) were considered in the assessment.

Each of the 721 precincts was classified according to ecozone (plains, mountains, or mixture of plains and mountains) and population density (urban or rural). The lifestyle and dietary habits of representative individuals in each type of precinct were obtained by means of focus-group sessions and interviews of key informants (Potischman et al. 2020). Doses were assessed to representative individuals defined by the important characteristics of four ethnic groups (Hispanics, Whites, Native Americans, and African Americans) and seven age groups (in utero, newborn, 1–2 y, 3–7 y, 8–12 y, 13–17 y, and adult).

Previous studies of fallout from nuclear weapons tests have shown that as a result of the preponderance of short-lived radionuclides, most of the dose from external irradiation

Table 18. Estimated probability distribution of the uncertainty in the dose (mGy Bq^{-1}) per unit intake for selected elements.[a]

Element	Reliability index	Uncertainty distribution around central estimates
Ba	Medium	TRI (0.5, 1, 1.5)
Ce	Low	TRI (0.3, 1, 1.5)
Cs	High	TRI (0.8, 1, 1.5)
I	High	TRI (0.8, 1, 1.5)
La	High	TRI (0.8, 1, 1.5)
Mo	Medium	TRI (0.5, 1, 1.5)
Np	Low	TRI (0.3, 1, 1.5)
Rh	Low	TRI (0.3, 1, 1.5)
Ru	Low	TRI (0.3, 1, 1.5)
Sr	High	TRI (0.8, 1, 1.5)
Te	Medium	TRI (0.5, 1, 1.5)
U	Low	TRI (0.3, 1, 1.5)
Y	Low	TRI (0.3, 1, 1.5)
Zr	Medium	TRI (0.5, 1, 1.5)

[a] The selected elements include the radionuclides that contributed to more than 95% of the internal dose to the organs and tissues considered in the study. For all other elements, the reliability index was judged to be low.

is delivered during a few months following a nuclear test (Beck 2005) while the annual doses from internal irradiation are much greater in the year following the test than in any subsequent year (Simon et al. 2010b). Thus, the doses from Trinity were calculated for only the first year following the day of the test (16 July 1945) for all 721 precincts, all four ethnicities, and all seven age groups.

The collection of models and parameter values presented here, enabling an assessment for multiple types of foods and modes of intake, make the Trinity study one of the most detailed assessments of exposure from nuclear testing fallout to have ever been conducted. There are, clearly, numerous uncertainties in the results of an assessment of an event so long in the past. However, the means for propagating the uncertainty of estimated doses are provided and uncertainties of doses have been estimated in a companion publication (Simon et al. 2020). The strategies and models presented here can be adapted to assessments of other nuclear events where radioactive fallout is a source of human exposure.

REFERENCES

Anspaugh LR, Simon SL, Gordeev KI, Likhtarev IA, Maxwell RM, Shinkarev SM. Movement of radionuclides in terrestrial ecosystems by physical processes. Health Phys 82:669–679; 2002.

Beck HL. Exposure rate conversion factors for radionuclides deposited on the ground. New York: US Department of Energy; Environmental Measurements Laboratory Report EML-378; 1980.

Beck HL. External dose estimates from NTS fallout. Appendix E, pages E-1 to E-57, in: Report on the feasibility of a study of the health consequences to the American population from nuclear weapons tests conducted by the United States and other nations. Washington, DC: US DHHS; 2005. Available at ***http://www.cdc.gov/nceh/radiation/fallout/default.htm***. Accessed 6 August 2020.

Beck HL. Estimates of H+12 Exposure Rates and Associated Uncertainty Received by the Population of Selected Villages in the Vicinity of the Semipalatinsk Test Site in Kazakhstan at the Time of the Semipalatinsk Test Site Atmospheric Tests (1949-1962). Application of Joint Russian/American Methodology for Fallout Dose Assessment to the Estimation of Internal Doses and Associated Uncertainty. Final Report to NCI in Fulfillment of PSC # HHSN 261200800397P. March 15, 2009.

Beck HL, Bouville A, Moroz BE, Simon SL. Fallout deposition in the Marshall Islands from Bikini and Enewetak nuclear weapons tests. Health Phys 99:124–142; 2010.

Beck HL, Simon SL, Bouville A, Romanyukha A. Accounting for unfissioned plutonium from the Trinity atomic bomb test. Health Phys 119:504–516; 2020.

Bellamy MB, Dewji SA, Leggett RW, Hiller M, Veinot K, Manger RP, Eckerman KF, Ryman JC, Easterly CE, Hertel NE, Stewart DJ. FGR 15. Federal Guidance Report No. 15: External Exposure to Radionuclides in Air, Water, and Soil. Washington, DC: U.S. Environmental Protection Agency, Office of Radiation and Indoor Air; Report EPA-402-R19-002; 2019.

Bouville A, Beck HL, Simon SL. Doses from external irradiation to Marshall Islanders from Bikini and Enewetak nuclear weapons tests. Health Phys 99:143–156; 2010.

Cahoon EK, Zhang R, Simon SL, Bouville A, Pfeiffer RM. Projected cancer risks to residents of New Mexico from exposure to Trinity radioactive fallout. Health Phys 119: 478–493; 2020.

Carini F. Radionuclides in plants bearing fruit. An overview. J Environ Radioact 46:77–97; 1999.

Cederwall R, Peterson K. Meteorological modeling of arrival and deposition of fallout at intermediate distances downwind of the Nevada Test Site. Health Phys 59:593–601; 1990.

Chamberlain AC. Interception and retention of radioactive aerosols by vegetation. Atmospheric Environment 4:57–78; 1970.

Chamberlain AC, Chadwick RC. Deposition of airborne radioiodine vapor. Nucleonics 8:22–25; 1953.

Church BW, Wheeler DL, Campbell CM, Nutley RV, Anspaugh LR. Overview of the Department of Energy's Off-Site Radiation Exposure Review Project. Health Phys 59:503–510; 1990.

Douglas RL. Levels and distribution of environmental plutonium around the TRINITY site. Las Vegas, NV: US Environmental Protection Agency, Office of Radiation Programs; Technical Note ORP/LV 78–3; 1978.

Dunning GM. Radiation from fallout and their effects. In: Eighty-fifth Congress First Session on The Nature of Radioactive Fallout from Nuclear Weapons Tests. Hearings before the Special Subcommittee on Radiation of the Joint Committee on Atomic Energy. Congress of the United States. Part I. Washington, DC: United States Government Printing Office; 1957: 170–196.

Gordeev K, Vasilenko I, Lebedev A, Bouville A, Luckyanov N, Simon SL, Stepanov Y, Shinkarev S, Anspaugh L. Fallout from nuclear tests: dosimetry in Kazakhstan. Radiat Environ Biophys 41:61–67; 2002.

Hansen WR, Rodgers JC. Radiological survey and evaluation of the fallout area from the TRINITY test: Chupadera Mesa and White Sands Missile Range, New Mexico. Los Alamos, NM: Los Alamos National Laboratory; Report LA-10256- MS; 1985.

Henderson RW. Approximation of the decay of fission and activation product mixtures. Los Alamos, NM: Los Alamos National Laboratory; Report LA-11968-MS; 1991.

Hicks HG. Calculation of the concentration of any radionuclide deposited on the ground by offsite fallout from a nuclear detonation. Health Phys 42:585–600; 1982.

Hicks HG. Results of calculations of external gamma radiation exposure rates from fallout and the related radionuclide compositions—the TRINITY event. Livermore, CA: University of California, Lawrence Livermore Laboratory; UCRL- 53705; 1985.

Hoffman FO, Thiessen KM, Frank ML, Blaylock BG. Quantification of the interception and initial retention of radioactive contaminants deposited on pasture grass by simulated rain. Atmospheric Environ 26A:3313–3321; 1992.

Hoffman FO, Thiessen KM, Rael RM. Comparison of interception and initial retention of wet-deposited contaminants leaves of different vegetation types. Atmospheric Environ 29:1771–1775; 1995.

Horton RE. Rainfall interception. Monthly Weather Rev 47: 608–623; 1919.

Ibrahim SA, Simon SL, Bouville A, Melo D, Beck HL. Alimentary tract absorption (f1 values) for radionuclides in local and regional fallout from nuclear tests. Health Phys 99:233–251; 2010.

International Atomic Energy Agency. Handbook of parameter values for the prediction of radionuclide transfer in terrestrial and freshwater environments. Vienna: IAEA; Technical Report Series No. 472; 2010.

International Commission on Radiological Protection. Age-dependent doses to members of the public from intake of radionuclides: Part 1. Oxford: Pergamon Press; ICRP Publication 56, Annals of the ICRP 20(2); 1989.

International Commission on Radiological Protection. Age-dependent doses to members of the public from intake of radionuclides: part 2—Ingestion dose coefficients. Oxford: Pergamon Press; ICRP Publication 67, Annals of the ICRP 23(3–4); 1993.

International Commission on Radiological Protection. Human respiratory tract model for radiological protection. Oxford: Pergamon Press; ICRP Publication 66, Annals of the ICRP 24(1–3); 1994.
International Commission on Radiological Protection. Age-dependent doses to members of the public from intake of radionuclides: part 4—inhalation dose coefficients. Oxford: Pergamon Press; ICRP Publication 71, Annals of the ICRP 25(3–4); 1995a.
International Commission on Radiological Protection. Age-dependent doses to members of the public from intake of radionuclides: part 3—ingestion dose coefficients. Oxford: Pergamon Press; ICRP Publication 69, Annals of the ICRP 25(1); 1995b.
International Commission on Radiological Protection. Corrected version, May 2002. Doses to the embryo and fetus from intakes of radionuclides by the mother. Oxford: Pergamon Press; Publication 88, Annals of the ICRP 31(1–3); 2001.
International Commission on Radiological Protection. Basic anatomical and physiological data for use in radiological protection: reference values. Oxford: Pergamon Press; Publication 89, Annals of the ICRP 32(3–4); 2002.
International Commission on Radiological Protection. Dose to infants from ingestion of radionuclides in mothers' milk. Oxford: Elsevier; Publication 95, Annals of the ICRP 34(3–4); 2004.
International Commission on Radiological Protection. Conversion coefficients for radiological protection quantities for external radiation exposures. Oxford: Elsevier Publication 116, Ann. ICRP 40(2–5); 2010.
Jacob P, Rosenbaum H, Petoussi N, Zankl M. Calculation of organ doses from environmental gamma rays using human phantoms and Monte-Carlo methods. Part II: radionuclides distributed in the air or deposited on the ground. Neuherberg: GSF-Institut für Strahlenschutz; GSF-Bericht 12/90; 1990.
Kinnersley RP, Scott LK. Aerial contamination of fruit through wet deposition and particulate dry deposition. J Environ Radioact 22:191–213; 2001.
Larson KH, Neel JW, Hawthorn HA, Mork HM, Rowland RH, Baurmash L, Lindberg RG, Olafson JH, Kowalewski BW. Distribution, characteristics, and biotic availability of fallout, Operation PLUMBBOB. Los Angeles, CA: University of California; WT-1488; 1966.
Lindberg RG, Romney EM, Olafson JH, Larson KH. Factors influencing the biological fate and persistence of radioactive fallout. Los Angeles, CA: University of California; WT-1177; 1959.
Maxwell RM, Anspaugh LR. An improved model for prediction of resuspension. Health Phys 101:722–730; 2011.
Menne MJ, Durre I, Vose RS, Gleason BE, Houston TG. An overview of the Global Historical Climatology Network—daily database. J Atmospheric Oceanic Technol 29:897–910; 2012. DOI: 10.1175/JTECH-D-11-00103.1.
Ministère de la Défense. La dimension radiologique des essais nucléaires français en Polynésie. Paris: République Française; 2006 (in French).
National Cancer Institute. Estimated exposures and thyroid doses received by the American people from iodine−131 in fallout following Nevada atmospheric nuclear bomb tests. Bethesda, MD: NCI; 1997.
National Council on Radiation Protection and Measurements. Uncertainties in the measurement and dosimetry of external radiation. NCRP Report No. 158; 2007.
National Council on Radiation Protection and Measurements. Radiation dose reconstruction: principles and practices. NCRP Report No. 163; 2009a.
National Council on Radiation Protection and Measurements. Uncertainties in internal radiation dose assessment. NCRP Report No. 164; 2009b.
National Council on Radiation Protection and Measurements. Deriving organ doses and their uncertainty for epidemiological studies. NCRP Report No. 178; 2018.
Ng YC, Anspaugh LR, Cederwall RT. ORERP internal dose estimates for individuals. Health Phys 59:693–713; 1990.
Potischman N, Salazar SI, Scott MA, Naranjo M, Haozous E, Bouville A, Simon SL. Methods and findings on diet and lifestyle used to support estimation of radiation doses from radioactive fallout from the Trinity nuclear test. Health Phys 119:390–399; 2020.
Pröhl G. Interception of dry and wet deposited radionuclides by vegetation. J Environ Radioact 100:675–682; 2009.
Quinn VE. Analysis of Nuclear Test TRINITY radiological and meteorological data. NOAA, Weather Service Nuclear Support Office, NVO 313; 1987.
Quinn VE. Analysis of meteorological and radiological data. Health Phys 59:577–592; 1990.
Sehmel GA. Particle and gas deposition: a review. Atmospheric Environ 14:981–1011; 1980.
Simmonds JR, Linsley GS. Parameters for modelling the interception and retention of deposits from atmosphere by grain and leafy vegetables. Health Phys 43:679–691; 1982.
Simon SL, Bouville A, Land C, Beck HL. Radiation doses and cancer risks in the Marshall Islands associated with exposure to radioactive fallout from Bikini and Enewetak nuclear weapons tests: summary. Health Phys 99:105–123; 2010a.
Simon SL, Bouville A, Melo D, Beck HL, Weinstock RM. Acute and chronic intakes of fallout radionuclides by Marshallese from nuclear weapons testing at Bikini and Enewetak and related internal radiation doses. Health Phys 99:157–200; 2010b.
Simon SL, Lloyd RD, Till JE, Hawthorne HA, Gren DC, Rallison ML, Stevens W. Development of a method to estimate thyroid dose from fallout radioiodine in a cohort study. Health Phys 59: 669–691; 1990.
Simon SL, Bouville A, Beck HL, Melo DR. Estimated radiation doses received by New Mexico residents from the 1945 Trinity nuclear test. Health Phys 119:428–477; 2020.
Thiessen KM, Hoffman FO. Trinity study dose assessment parameters—final report to the National Cancer Institute. Oak Ridge, TN: Oak Ridge Center for Risk Analysis, Inc.; 2018.
Thompson CB, McArthur ED, Hutchinson SW. Development of the Town Data Base: estimates of exposure rates and times of fallout arrival near the Nevada Test Site. Las Vegas, NV: US Department of Energy Nevada Operations Office; Report DOE/NV-374; 1994.
United Nations Scientific Committee on the Effects of Atomic Radiation. UNSCEAR 1993 Report. Sources and effects of ionizing radiation. Annex B: Exposures from man-made sources of radiation. New York: United Nations; 1993.
US Department of Health and Human Services. A report on the feasibility of a study on the health consequences to the American population from nuclear weapons tests conducted by the United States and other nations. Prepared for the U.S. Congress. Washington, DC: US DHHS; 2005. Available at ***http://www.cdc.gov/nceh/radiation/fallout/default.htm***. Accessed 6 August 2020.
Vandecasteele CM, Baker S, Förstel H, Musinsky M, Millan R, Madoz-Escande C, Tormos J, Sauras T, Schulte E, Colle C. Interception, retention and translocation under greenhouse conditions of radiocaesium and radiostrontium from a simulated accidental source. Sci Total Environ 278:199–214; 2001.

■■